

Supporting Information

Continuous Flash Sublimation of Inorganic Halide Perovskites: Overcoming Rate and Continuity Limitations of Vapor Deposition

Tobias Abzieher, Christopher P. Muzzillo, Mirzo Mirzokarimov, Gabriella Lahti, Wylie F. Kau, Daniel M. Kroupa, Spencer G. Cira, Hugh W. Hillhouse, Ahmad R. Kirmani, Jackson Schall, Dana Kern, Joseph M. Luther, and David T. Moore

Tab. S1: Summary of key characteristics of vapor-processed *hybrid* perovskite materials for solar cell applications. Only the best reported devices from each publication and only those with accessible deposition rates are reported here. Solar cell parameters shown here represent values extracted from the reverse *J-V* scan. Data is presented visually in Figure 1 in the main manuscript.

authors	year	absorber composition	deposition approach	deposition rate (nm min ⁻¹)	source of rate	PCE (%)	FF (%)	V _{oc} (V)	J _{sc} (mA cm ⁻²)	reference
Liu et al.	2013	MAPb(I _{1-x} Cl _x) ₃	co-evaporation	2.6	in article	15.4	67.0	1.07	21.5	[1]
Leyden et al.	2014	MAPb(I _{1-x} Cl _x) ₃	CVD	2.4	in article	11.8	n/a	n/a	n/a	[2]
Chen et al.	2014	MAPb(I _{1-x} Cl _x) ₃	layer-by-layer	4.1	from authors	15.4	72.2	1.02	20.9	[3]
Ono et al.	2014	MAPb(I _{1-x} Cl _x) ₃	co-evaporation	4.2	in article	9.9	53.5	1.09	17.0	[4]
Roldán-Carmona et al.	2014	MAPbI ₃	co-evaporation	4.3	from authors	7.0	47.0	1.04	14.3	[5]
Momblona et al.	2014	MAPbI ₃	co-evaporation	4.8	from authors	12.7	63.0	1.07	18.8	[6]
Malinkiewicz et al.	2014	MAPbI ₃	co-evaporation	4.8	from authors	12.0	67.0	1.05	16.1	[7]
Malinkiewicz et al.	2014	MAPbI ₃	co-evaporation	5.0	from authors	14.8	75.0	1.09	18.2	[8]
Polander et al.	2014	MAPb(I _{1-x} Cl _x) ₃	co-evaporation	5.6	from authors	10.9	70.0	0.97	16.1	[9]
Ng et al.	2014	MAPb(I _{1-x} Cl _x) ₃	co-evaporation	6.8	from authors	6.1	60.0	0.82	12.5	[10]
Subbiah et al.	2014	MAPb(I _{1-x} Cl _x) ₃	co-evaporation	10.4	in article	7.3	75.0	0.94	14.9	[11]
Hu et al.	2014	MAPbI ₃	layer-by-layer	11.7	in article	5.4	50.0	0.80	13.6	[12]
Abbas et al.	2015	MAPbI ₃	layer-by-layer	1.9	in article	13.7	65.3	0.96	21.8	[13]
Teuscher et al.	2015	MAPbI ₃	co-evaporation	1.9	in article	12.5	n/a	n/a	n/a	[14]
Wang et al.	2015	MAPbI ₃	layer-by-layer	2.0	in article	11.5	52.4	1.10	19.9	[15]
Tavakoli et al.	2015	MAPbI ₃	CVD	3.0	in article	9.2	61.0	0.95	15.9	[16]

authors	year	absorber composition	deposition approach	deposition rate (nm min ⁻¹)	source of rate	PCE (%)	FF (%)	V _{oc} (V)	J _{sc} (mA cm ⁻²)	reference
Leyden <i>et al.</i>	2015	FAPb(I _{1-x} Cl _x) ₃	CVD	3.3	in article	12.5	59.0	0.98	21.5	[17]
Luo <i>et al.</i>	2015	MAPbI ₃	CVD	3.7	in article	12.7	64.5	0.91	21.7	[18]
Tavakoli <i>et al.</i>	2015	MAPb(I _{1-x} Cl _x) ₃	CVD	5.0	in article	11.1	64.0	0.97	18.0	[16]
Yang <i>et al.</i>	2015	MAPb(I _{1-x} Cl _x) ₃	layer-by-layer	6.8	from authors	16.0	72.0	1.00	22.3	[19]
Ng <i>et al.</i>	2015	MAPbI ₃	layer-by-layer	15.8	from authors	12.5	60.0	0.96	21.8	[20]
Longo <i>et al.</i>	2015	MAPbI ₃	single-source evaporation	1,000.0	from authors	12.2	68.0	1.07	18.0	[21]
Leyden <i>et al.</i>	2016	MAPbI ₃	CVD	3.4	in article	15.6	68.0	1.06	21.7	[22]
Leyden <i>et al.</i>	2016	FAPbI ₃	CVD	3.4	in article	10.4	53.0	1.02	19.5	[22]
Hsiao <i>et al.</i>	2016	MAPbI ₃	co-evaporation	4.0	in article	17.6	73.2	1.06	22.7	[23]
Kim <i>et al.</i>	2016	MAPbI ₃	co-evaporation	4.7	in article	14.5	72.0	1.00	20.1	[24]
Momblona <i>et al.</i>	2016	MAPbI ₃	co-evaporation	4.8	from authors	20.3	80.5	1.14	22.1	[25]
Fan <i>et al.</i>	2016	MAPbI ₃	single-source evaporation	133.3	in article	10.8	60.0	0.93	19.4	[26]
Xu <i>et al.</i>	2016	MAPbI ₃	single-source evaporation	2,500.0	in article	10.0	64.0	0.99	15.8	[27]
Borchert <i>et al.</i>	2017	FAPbI ₃	co-evaporation	3.1	from authors	15.8	70.8	1.01	22.1	[28]
Forgács <i>et al.</i>	2017	MAPbI ₃	co-evaporation	4.5	from authors	19.1	81.6	1.07	21.8	[29]
Forgács <i>et al.</i>	2017	Cs _{0.15} FA _{0.85} Pb(I _{0.3} Br _{0.7}) ₃	co-evaporation	4.5	from authors	10.7	77.8	1.20	11.4	[29]
Patel <i>et al.</i>	2017	MAPbI ₃	co-evaporation	4.9	in article	15.8	75.0	1.04	20.2	[30]
Zhu <i>et al.</i>	2017	Cs _{0.23} MA _{0.77} PbI ₃	co-evaporation	10.0	from authors	20.1	79.0	1.10	23.2	[31]
Tavakoli <i>et al.</i>	2017	MAPbI ₃	layer-by-layer	17.5	in article	15.9	83.0	0.96	20.1	[32]

authors	year	absorber composition	deposition approach	deposition rate (nm min ⁻¹)	source of rate	PCE (%)	FF (%)	V _{oc} (V)	J _{sc} (mA cm ⁻²)	reference
Cojocaru <i>et al.</i>	2018	MAPbI ₃	co-evaporation	4.2	in article	17.1	75.0	1.01	21.3	[33]
Longo <i>et al.</i>	2018	MAPbI ₃	co-evaporation	5.0	from authors	17.4	81.2	1.09	19.6	[34]
Longo <i>et al.</i>	2018	MAPb(I _{0.8} Br _{0.2}) ₃	co-evaporation	5.0	from authors	15.6	81.9	1.10	17.3	[34]
Pérez-del-Rey <i>et al.</i>	2018	MAPbI ₃	co-evaporation	5.9	from authors	20.8	82.1	1.16	21.9	[35]
Gil-Escríg <i>et al.</i>	2018	Cs _{0.5} FA _{0.4} MA _{0.1} Pb(I _{0.83} Br _{0.17}) ₃	co-evaporation	6.2	from authors	16.0	82.0	1.15	17.0	[36]
Gil-Escríg <i>et al.</i>	2018	Cs _{0.5} FA _{0.5} Pb(I _{0.83} Br _{0.17}) ₃	co-evaporation	6.2	from authors	8.5	57.0	0.85	17.6	[36]
Luo <i>et al.</i>	2018	Cs _{0.24} FA _{0.76} Pb(I _{1-x} Br _x) ₃	layer-by-layer	15.7	from authors	17.3	71.0	1.07	22.9	[37]
Luo <i>et al.</i>	2018	FAPb(I _{1-x} Br _x) ₃	layer-by-layer	25.0	from authors	11.3	65.0	1.00	17.4	[37]
Tai <i>et al.</i>	2018	MAPbI ₃	single-source evaporationt	3,000.0	from authors	16.8	75.0	0.98	23.1	[38]
Abzieher <i>et al.</i>	2019	MAPbI ₃	co-evaporation	2.3	from authors	15.6	72.0	1.06	20.3	[39]
Abzieher <i>et al.</i>	2019	MAPbI ₃	co-evaporation	2.4	from authors	16.8	79.0	1.03	20.7	[40]
Borchert <i>et al.</i>	2019	MAPbI ₃	co-evaporation	2.5	in article	15.0	n/a	n/a	n/a	[41]
Qiu <i>et al.</i>	2019	Cs _{0.1} FA _{0.9} Pb(I _{0.97} Br _{0.03}) ₃	layer-by-layer	2.5	from authors	13.3	73.2	0.90	20.2	[42]
La-Placa <i>et al.</i>	2019	MAPbI ₃	co-evaporation	4.5	from authors	18.9	78.5	1.06	22.7	[43]
Kottokkaran <i>et al.</i>	2019	MAPbI ₃	co-evaporation	4.7	from authors	17.4	77.0	1.03	22.0	[44]
Ball <i>et al.</i>	2019	Cs _{1-x} FA _x Pb _{1-y} Sn _y I ₃	co-evaporation	5.1	in article	11.5	74.0	0.78	20.3	[45]
Pérez-del-Rey <i>et al.</i>	2019	MAPbI ₃	co-evaporation	5.9	from authors	19.3	79.3	1.10	22.0	[46]
Palazon <i>et al.</i>	2019	MAPbI ₃	co-evaporation	6.6	from authors	19.7	81.2	1.16	20.8	[47]
Kiermasch <i>et al.</i>	2019	MAPbI ₃	co-evaporation	6.8	from authors	18.2	72.0	1.11	22.7	[48]

authors	year	absorber composition	deposition approach	deposition rate (nm min ⁻¹)	source of rate	PCE (%)	FF (%)	V _{oc} (V)	J _{sc} (mA cm ⁻²)	reference
Lin <i>et al.</i>	2019	MAPbI ₃	layer-by-layer	9.1	in article	17.3	72.4	1.01	23.7	[49]
Hoerantner <i>et al.</i>	2019	MAPbI ₃	layer-by-layer	13.5	in article	6.9	48.0	1.01	14.2	[50]
Arivazhagan <i>et al.</i>	2019	MAPbI ₃	co-evaporation	17.5	in article	15.7	66.8	1.08	21.8	[51]
Tavakoli <i>et al.</i>	2019	FA _{1-x} MA _x Pb(I _{1-y} Cl _y) ₃	layer-by-layer	24.5	in article	17.7	75.0	1.04	22.7	[52]
Peng <i>et al.</i>	2019	MAPbI ₃	single-source evaporation	36.0	in article	2.6	34.0	0.77	10.0	[53]
Zheng <i>et al.</i>	2019	BA ₂ MA ₃ Pb ₄ I ₁₃	single-source evaporation	400.0	from authors	2.5	45.8	0.85	6.5	[54]
Qiu <i>et al.</i>	2020	Cs _{1-x} FA _x PbI ₃	CVD	1.6	in article	7.6	42.1	0.96	19.0	[55]
Ngqoloda <i>et al.</i>	2020	MAPbI ₃	CVD	1.8	in article	11.7	59.5	0.88	22.4	[56]
Hellmann <i>et al.</i>	2020	MAPbI ₃	co-evaporation	2.1	from authors	13.7	n/a	1.03	19.4	[57]
Harding <i>et al.</i>	2020	MAPbI ₃	layer-by-layer	2.6	in article	12.1	56.6	0.98	21.9	[58]
Lohmann <i>et al.</i>	2020	MAPbI ₃	co-evaporation	2.9	in article	18.3	77.8	1.08	21.7	[59]
Li <i>et al.</i>	2020	MAPbI ₃	co-evaporation	4.3	from authors	19.1	76.4	1.12	22.3	[60]
Roß <i>et al.</i>	2020	MAPbI ₃	co-evaporation	5.0	in article	20.3	79.0	1.15	22.4	[61]
Gil-Escríg <i>et al.</i>	2020	FA _{1-x} MA _x PbI ₃	co-evaporation	5.6	from authors	18.8	76.0	1.09	22.6	[62]
Babaei <i>et al.</i>	2020	MAPb(I _{1-x} Cl _x) ₃	co-evaporation	5.6	from authors	16.1	73.0	1.13	19.5	[63]
Kim <i>et al.</i>	2020	MAPbI ₃	co-evaporation	5.6	from authors	18.7	n/a	n/a	n/a	[64]
Li <i>et al.</i>	2020	MAPbI ₃	co-evaporation	5.8	in article	20.3	77.7	1.12	23.3	[65]
Zanoni <i>et al.</i>	2020	MAPbI ₃	co-evaporation	6.6	from authors	18.0	78.3	1.12	20.3	[66]
Babaei <i>et al.</i>	2020	MAPbI ₃	co-evaporation	6.7	from authors	18.4	n/a	n/a	n/a	[67]

authors	year	absorber composition	deposition approach	deposition rate (nm min ⁻¹)	source of rate	PCE (%)	FF (%)	V _{oc} (V)	J _{sc} (mA cm ⁻²)	reference
Igual-Muñoz <i>et al.</i>	2020	FAPb _{0.5} Sn _{0.5} I ₃	co-evaporation	7.6	from authors	14.0	79.3	0.72	24.5	[68]
Chiang <i>et al.</i>	2020	Cs _{0.3} FA0.7Pb(I _{0.9} Br _{0.1}) ₃	co-evaporation	8.2	from authors	18.1	74.6	1.06	23.0	[69]
Ji <i>et al.</i>	2020	Cs _{0.1} FA _{0.9} Pb(I _{0.97} Br _{0.03}) ₃	co-evaporation	10.0	from authors	16.6	79.7	1.07	19.5	[70]
Lei <i>et al.</i>	2020	MAPbI ₃	layer-by-layer	11.4	in article	19.2	80.9	1.06	22.4	[71]
Qiu <i>et al.</i>	2020	Cs _{1-x} FA _x PbI ₃	CVD	37.0	in article	15.5	70.2	0.99	22.3	[55]
Smecca <i>et al.</i>	2021	MAPbI ₃	layer-by-layer	1.7	in article	17.5	75.4	1.07	21.6	[72]
Sahli <i>et al.</i>	2021	MAPbI ₃	CVD	2.0	in article	12.3	n/a	n/a	n/a	[73]
Choi <i>et al.</i>	2021	MAPbI ₃	layer-by-layer	3.8	from authors	18.5	79.0	1.07	21.9	[74]
Li <i>et al.</i>	2021	MAPbI ₃	co-evaporation	4.2	from authors	20.6	82.4	1.12	22.3	[75]
Li <i>et al.</i>	2021	MAPbI ₃	co-evaporation	4.2	in article	20.6	82.4	1.12	22.3	[75]
Li <i>et al.</i>	2021	MAPbI ₃	co-evaporation	4.2	in article	19.3	80.3	1.11	21.7	[75]
Dewi <i>et al.</i>	2021	MAPbI ₃	co-evaporation	4.6	in article	17.2	74.6	1.06	21.7	[76]
Paliwal <i>et al.</i>	2021	MAPbI ₃	co-evaporation	4.9	from authors	13.0	76.5	1.12	15.2	[77]
Susic <i>et al.</i>	2021	MAPbI ₃	co-evaporation	5.0	from authors	18.3	76.0	1.1	21.9	[78]
Gil-Escríg <i>et al.</i>	2021	MAPbI ₃	co-evaporation	5.6	from authors	18.2	78.0	1.12	20.9	[79]
Klipfel <i>et al.</i>	2021	MAPbI ₃	co-evaporation	5.6	in article	15.2	77.4	0.98	19.9	[80]
Gallet <i>et al.</i>	2021	MAPbI ₃	co-evaporation	5.6	from authors	14.7	77.0	1.05	18.2	[81]
Roß <i>et al.</i>	2021	FA _{0.53} MA _{0.47} PbI ₃	co-evaporation	6.3	in article	20.4	75.9	1.05	25.7	[82]
Roß <i>et al.</i>	2021	FAPbI ₃	co-evaporation	6.5	in article	15.8	n/a	n/a	n/a	[82]

authors	year	absorber composition	deposition approach	deposition rate (nm min ⁻¹)	source of rate	PCE (%)	FF (%)	V _{oc} (V)	J _{sc} (mA cm ⁻²)	reference
Kaya <i>et al.</i>	2021	MAPbI ₃	co-evaporation	6.7	from authors	19.2	79.7	1.09	22.1	[83]
Feng <i>et al.</i>	2021	Cs _{1-x} FA _x PbI ₃	layer-by-layer	6.8	from authors	21.3	77.2	1.11	24.9	[84]
Gil-Escriv <i>et al.</i>	2021	Cs _{0.35} FA _{0.65} Pb(I _{0.73} Br _{0.27}) ₃	co-evaporation	7.7	from authors	16.8	79.0	1.18	18.0	[85]
Abzieher <i>et al.</i>	2021	MAPbI ₃	co-evaporation	9.3	from authors	19.5	83.0	1.08	21.6	[86]
Ritzer <i>et al.</i>	2021	MAPbI ₃	co-evaporation	9.3	from authors	19.2	82.0	1.08	21.6	[87]
Lin <i>et al.</i>	2021	AL _{1-x} MA _x PbI ₃	layer-by-layer	14.3	from authors	18.2	74.8	1.08	22.6	[88]
Lin <i>et al.</i>	2021	MAPbI ₃	layer-by-layer	14.3	from authors	17.2	72.7	1.05	22.6	[88]
Kroll <i>et al.</i>	2022	Cs _{1-x} FA _x Pb(I _{1-y} Br _y) ₃	co-evaporation	6.0	in article	15.6	76.6	1.09	18.7	[89]
Li <i>et al.</i>	2022	Cs _{0.05} FA _{0.95} Pb(I _{1-x} Cl _x) ₃	layer-by-layer	11.2	from authors	24.4	81.8	1.15	25.9	[90]

[†] processes are batch processes that rely on solution-based fabrication steps, MA: methylammonium (CH₃NH₃⁺), FA: formamidinium (CH(NH₂)₂⁺), BA: butylammonium (C₄H₁₂N⁺), AL: anilinium (C₆H₅NH₃⁺)

Tab. S2: Summary of key characteristics of vapor-processed *inorganic* perovskite materials for solar cell applications. Only the best reported devices from each publication and only those with accessible deposition rates are reported here. Solar cell parameters shown here represent values extracted from the reverse J - V scan. Data is presented visually in Figure 1 in the main manuscript.

authors	year	absorber composition	deposition approach	deposition rate (nm min ⁻¹)	source of rate	PCE (%)	FF (%)	V_{oc} (V)	J_{sc} (mA cm ⁻²)	reference
Ma <i>et al.</i>	2016	CsPbI ₂	co-evaporation	2.2	from authors	4.7	56.0	0.96	8.7	[91]
Moghe <i>et al.</i>	2016	CsSn(Br _{1-x} F _x) ₃	layer-by-layer	2.8	in article	0.6	n/a	n/a	n/a	[92]
Ma <i>et al.</i>	2017	CsPbI ₂ Br	co-evaporation	1.5	from authors	7.7	67.0	1.01	11.5	[93]
Shahiduzzaman <i>et al.</i>	2017	CsPbI ₃	layer-by-layer	2.4	in article	6.8	72.0	0.79	12.1	[94]
Hutter <i>et al.</i>	2017	CsPbI ₃	layer-by-layer	5.2	from authors	8.8	68.0	1.00	13.0	[95]
Chen <i>et al.</i>	2017	CsPbI ₂ Br	co-evaporation	11.4	from authors	11.8	68.0	1.13	15.2	[96]
Chen <i>et al.</i>	2017	CsPbI ₃	co-evaporation	12.0	from authors	9.4	56.0	0.98	17.3	[96]
Chen <i>et al.</i>	2018	Cs ₂ TiBr ₆	layer-by-layer	0.3	in article	3.3	56.0	1.02	5.7	[97]
Lei <i>et al.</i>	2018	CsPbBr ₃	co-evaporation	5.0	from authors	7.0	78.5	1.27	7.0	[98]
Kottokkaran <i>et al.</i>	2018	CsPbI ₃	layer-by-layer	5.3	from authors	9.5	65.0	0.95	14.9	[99]
Li <i>et al.</i>	2018	CsPbBr ₃	layer-by-layer	5.7	in article	8.3	75.9	1.30	8.5	[100]
Park <i>et al.</i>	2018	CsPbI ₂ Br	co-evaporation	14.8	in article	5.7	49.0	1.10	10.9	[101]
Chen <i>et al.</i>	2018	CsPbBr ₃	co-evaporation	22.5	from authors	7.8	77.1	1.44	7.0	[102]
Fan <i>et al.</i>	2019	Cs ₂ AgBiBr ₆	single-source evaporation	1.9	in article	0.7	65.0	0.87	1.2	[103]
Tong <i>et al.</i>	2019	CsPbBr ₃	layer-by-layer	3.0	in article	10.9	74.5	1.50	9.8	[104]
Chen <i>et al.</i>	2019	CsPbBr ₃	layer-by-layer	3.0	from authors	9.0	73.1	1.44	8.5	[105]

authors	year	absorber composition	deposition approach	deposition rate (nm min ⁻¹)	source of rate	PCE (%)	FF (%)	V _{oc} (V)	J _{sc} (mA cm ⁻²)	reference
Lin <i>et al.</i>	2019	CsPbI ₂ Br	layer-by-layer	6.7	in article	13.0	74.0	1.13	15.6	[106]
Becker <i>et al.</i>	2019	CsPbI ₃	co-evaporation	7.3	from authors	12.5	73.0	0.96	17.8	[107]
Liu <i>et al.</i>	2019	CsPbBr ₃	layer-by-layer	33.3	in article	7.6	75.2	1.33	7.6	[108]
Zhang <i>et al.</i>	2019	CsPbBr ₃	layer-by-layer	36.5	from authors	8.9	80.4	1.52	7.2	[109]
Tai <i>et al.</i>	2019	CsPbI ₂ Br	single-source evaporation [†]	2,500.0	from authors	12.2	72.0	1.10	15.4	[110]
Li <i>et al.</i>	2020	CsPbBr ₃	single-source evaporation	3.6	in article	8.7	81.0	1.37	7.8	[111]
Gaonkar <i>et al.</i>	2020	CsPb(I _{1-x} Br _x) ₃	layer-by-layer	5.7	from authors	11.8	n/a	n/a	n/a	[112]
Mi <i>et al.</i>	2020	CsPbBr ₃	layer-by-layer	6.3	in article	7.1	73.0	1.36	7.2	[113]
Igual-Muñoz <i>et al.</i>	2020	CsPbI ₂ Br	co-evaporation	11.9	in article	10.0	73.1	0.96	14.3	[114]
Xiang <i>et al.</i>	2020	CsPbBr ₃	layer-by-layer	30.0	from authors	9.4	82.2	1.55	7.4	[115]
Hua <i>et al.</i>	2020	CsPbBr ₃	layer-by-layer	30.0	from authors	7.2	79.0	1.42	6.5	[116]
Abib <i>et al.</i>	2021	Cs(Sn _{1-x} Pb _x)Br ₃	single-source evaporation	3.0	in article	9.0	71.0	1.36	9.3	[117]
Duan <i>et al.</i>	2021	CsPbBr ₃	co-evaporation	5.9	from authors	9.4	71.3	1.35	9.8	[118]
Liu <i>et al.</i>	2022	CsPbBr ₃	single-source evaporation	31.0	in article	7.8	80.0	1.43	6.8	[119]
Abzieher <i>et al.</i>	2022	CsPb(I _{0.75} Br _{0.25}) ₃	single-source evaporation	84.4	In article	13.8	77.1	1.18	15.2	this work
Abzieher <i>et al.</i>	2022	CsPb(I _{0.83} Br _{0.17}) ₃	single-source evaporation	84.4	In article	14.9	76.0	1.17	16.8	this work
Abzieher <i>et al.</i>	2022	CsPb(I _{0.83} Br _{0.17}) ₃	single-source evaporation	95.0	In article	14.1	71.6	1.15	17.1	this work
Abzieher <i>et al.</i>	2022	CsPbI ₂ Br	single-source evaporation	116.7	In article	12.8	77.7	1.15	14.3	this work
Abzieher <i>et al.</i>	2022	CsPb(I _{0.83} Br _{0.17}) ₃	single-source evaporation	134.3	In article	13.4	72.1	1.14	16.3	this work

[†] processes are batch processes that rely on solution-based fabrication steps

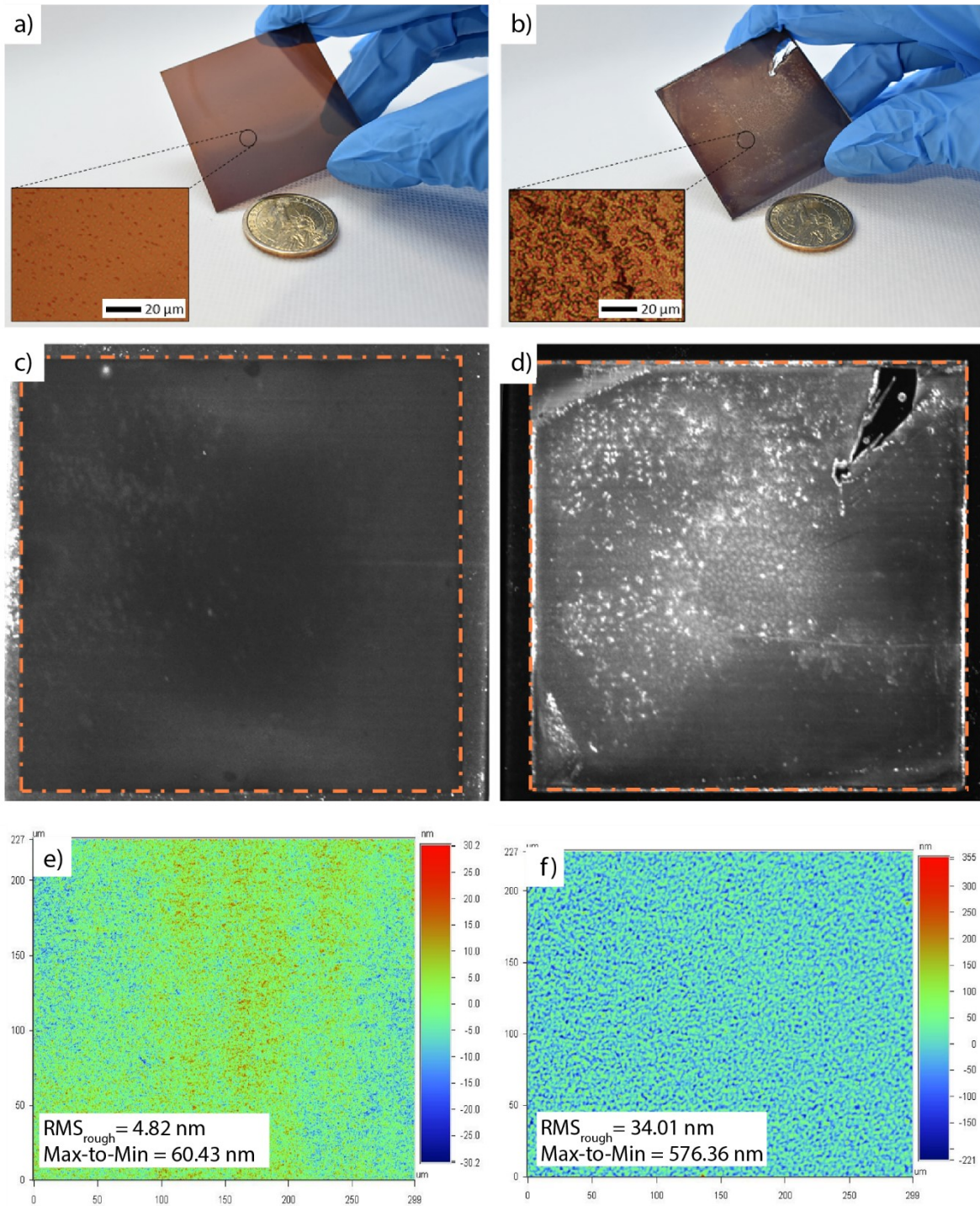


Fig. S1: Large-area deposition of a $\text{CsPb}(\text{I}_{0.67}\text{Br}_{0.33})_3$ thin films prepared by continuous flash sublimation (a) and spin casting (b) on a $2'' \times 2''$ substrate. The insets show microscope images of the surface of both thin films. Strong macroscopic as well as microscopic inhomogeneities are observed for the spin-casted thin film, which are related to the complex solvent extraction, nucleation, and phase stabilization mechanism in inorganic halide perovskite materials prepared by solution-based approaches. In contrast, a high uniformity is achieved for the vapor processed thin film. In addition, the high visual uniformity directly translates into a good homogeneity of

the opto-electronic properties as shown in a comparison of PL maps and surface roughness between the flash sublimed (c and e) and solution-processed (d and f) large-area thin films. Minor inhomogeneities in the flash sublimed film are believed to arise from dirtying of the substrate resulting in small variations during crystallization. The spin casted film was prepared by dissolving PbI_2 , PbBr_2 , and CsI stoichiometrically in DMF:DMSO (volume ratio: 4:1) to get a 1.2M solution. Spin coating was performed in a two-step approach consisting of step at 1,000 rpm for 10 sec followed by a step at 3,000 rpm for 30 sec. The film was then dried for 2 min at 50 °C and annealed for 1 min at 300 °C. Profilometry images are $300 \mu\text{m} \times 227 \mu\text{m}$, images were taken at 5 points across the large area films, image shown is the image that most closely matches the average RMS_{roughness} for all 5 points.

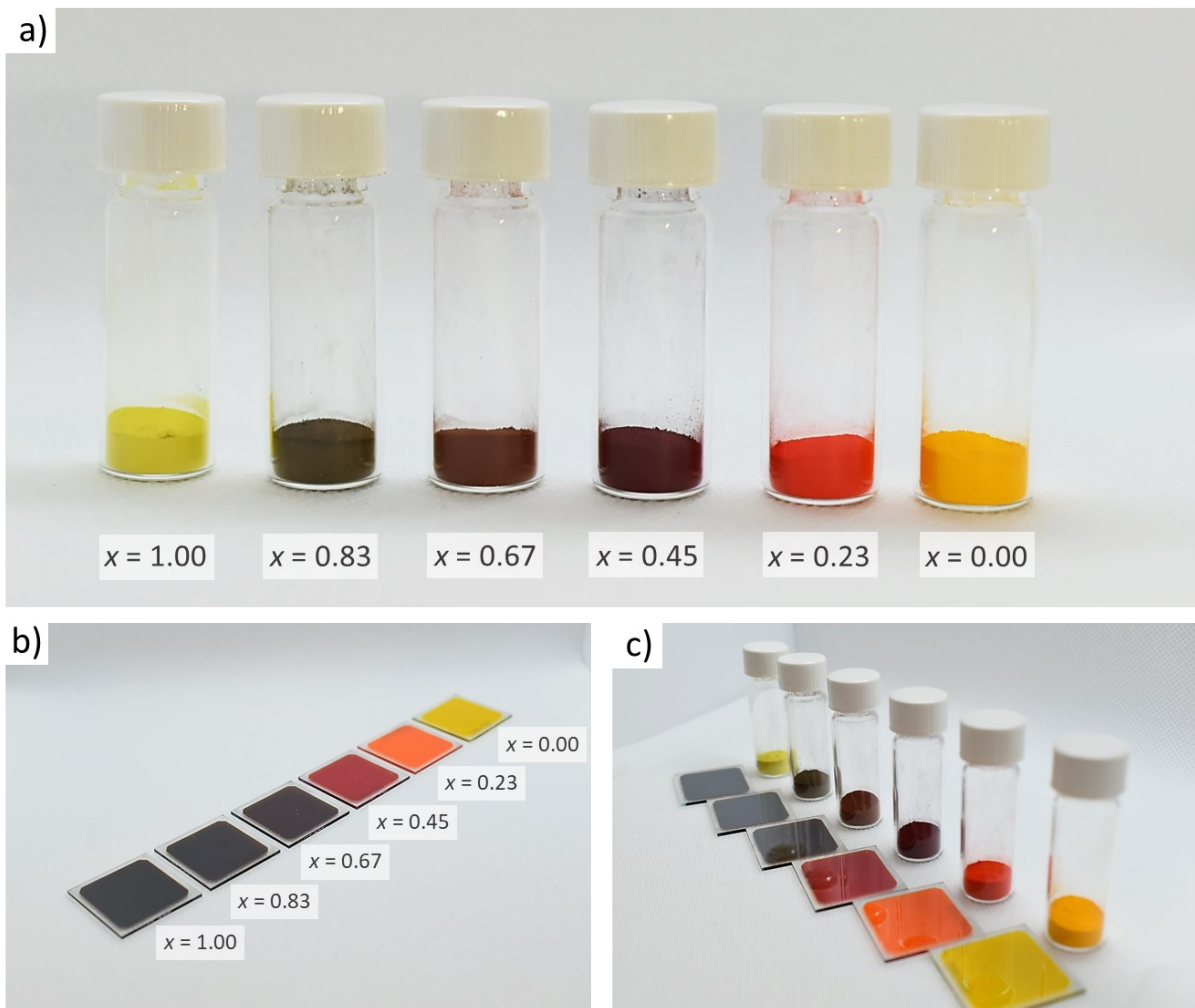


Fig. S2: Photographs of mechano-chemically synthesized inorganic halide perovskite powders (a, c) and thin films prepared with these powders (b, c). All powders have a stoichiometric composition following the formula $\text{CsPb}(\text{I}_x\text{Br}_{1-x})_3$. The visual appearance of the powder with iodine contents $x = 1.00$ clearly indicates the formation of the photoinactive hexagonal phase (yellow phase). Lowering the iodine content results in a partly (e.g., for powders with an iodine content of $x = 0.83$ and $x = 0.67$ with their green or light brown occurrence) or fully (e.g., for powders with iodine contents $x > 0.67$) occurrence of the photoactive perovskite phase already in the powder. All thin films based on these mechano-chemically synthesized powders are characterized by their high lateral uniformity as well as the occurrence of the photoactive phase.

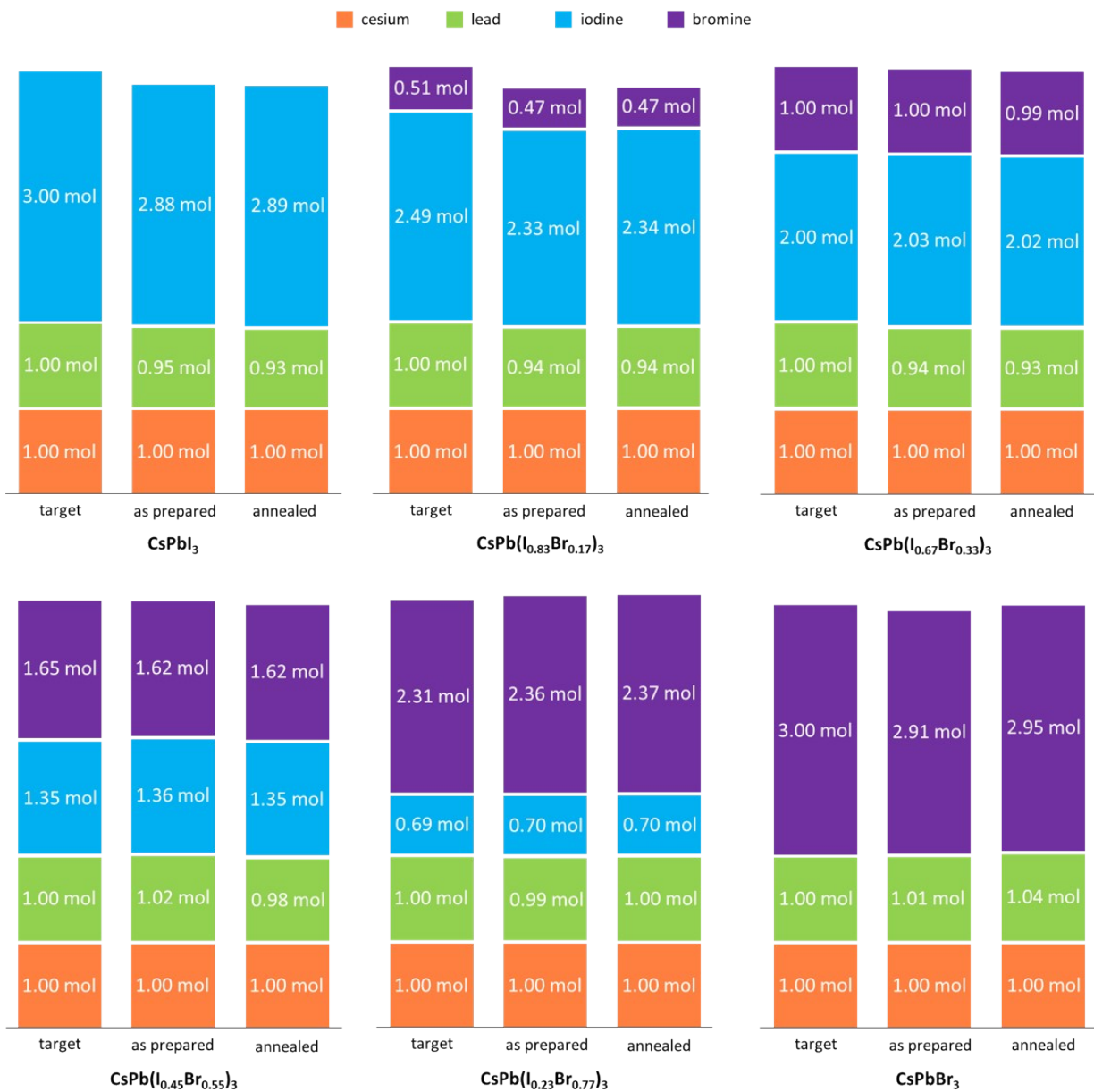


Fig. S3: Inductively coupled plasma mass spectrometry (ICP-MS) analysis of the composition of thin films prepared by CFS of mechano-chemically synthesized source powders with different iodine-to-bromine ratios. All thin films exhibit the expected composition of stoichiometric source powder indicating a direct compositional transition from powder to thin film, thus, a deposition within the flash sublimation regime. In addition, post annealing does not change the general composition of the thin films. All molar ratios have been normalized to the cesium values. The expected error of the measurement is in the range of $\pm 5\%$ _{rel}.

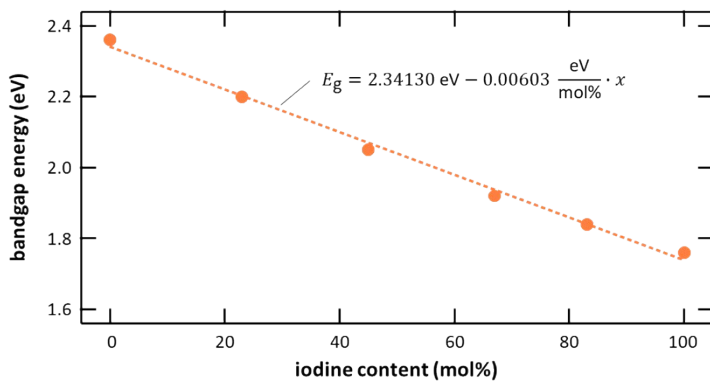


Fig. S4: Bandgap energy trend with varying iodine content for the inorganic material system $\text{CsPb}(\text{I}_x\text{Br}_{1-x})_3$. In first approximation, the trend curve follows a linear trend as expected for a substitutional solid solution of iodine and bromine. The linear fitting formula is used for the calculation of bandgap energies throughout this work.

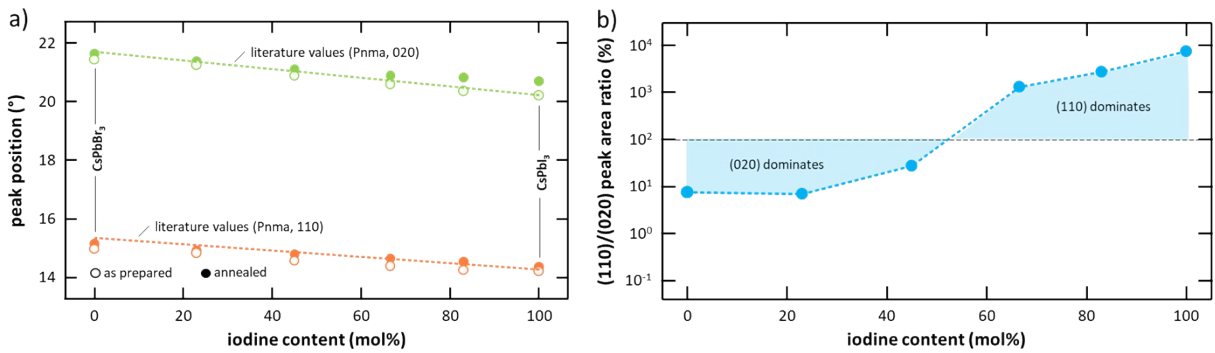


Fig. S5: Crystallographic properties of inorganic halide perovskite thin films with different iodine-to-bromine ratios prepared by CFS. (a) Peak position of the (110) and (020) diffraction peak for as-prepared (open circles) and annealed (full circles) with varying iodine-to-bromine ratio. Peak positions follow a linear trend when replacing iodine by bromine. The dashed lines represent the theoretical values expected for the orthorhombic crystal phase (Pnma). A small shift to larger diffraction angles is observed for all samples after annealing. (b) Preferred crystal orientation based on the ratio of the peak areas of the (110) and (020) peaks. A change in preferred crystal orientation is observed when the iodine content is varied. All values have been extracted from X-ray diffractograms shown in the main manuscript. Samples for XRD were deposited on top of glass/ITO/SnO₂ substrates.

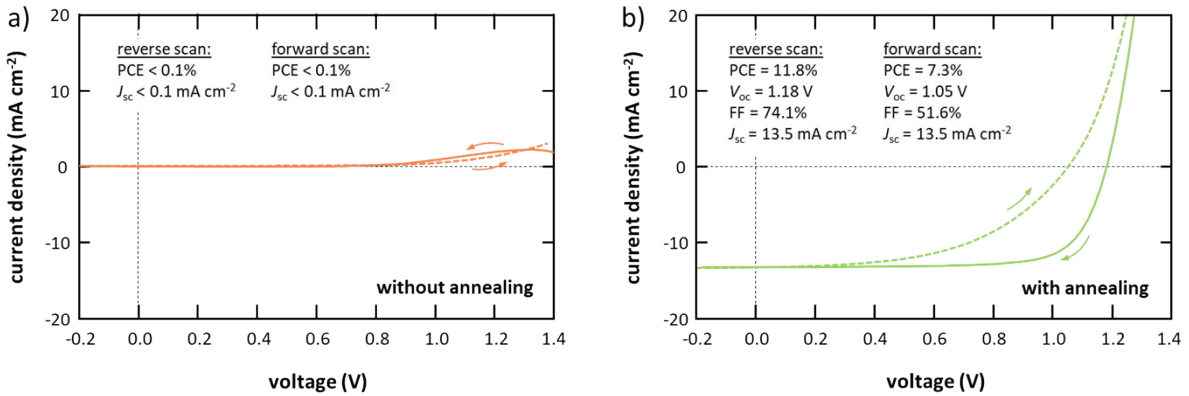


Fig. S6: Influence of post-annealing procedure on the performance of solar cells employing a $\text{CsPb}(\text{I}_{0.67}\text{Br}_{0.33})_3$ absorber. (a) Solar cell whose absorber did not undergo a post-annealing step and (b) solar cell whose absorber underwent a post-annealing step in inert atmosphere at a temperature of $330 \text{ }^\circ\text{C}$ for 1 min. Without post annealing, the absorber does not generate a considerable amount of extractable charge carriers, thus, also does not result in a notable open-circuit voltage. To circumvent the need for oxidation, the hole transport layers in these devices were doped with a cobalt TFSI salt which, however, increases hysteresis significantly (see Figure S11 in the Supporting Information).

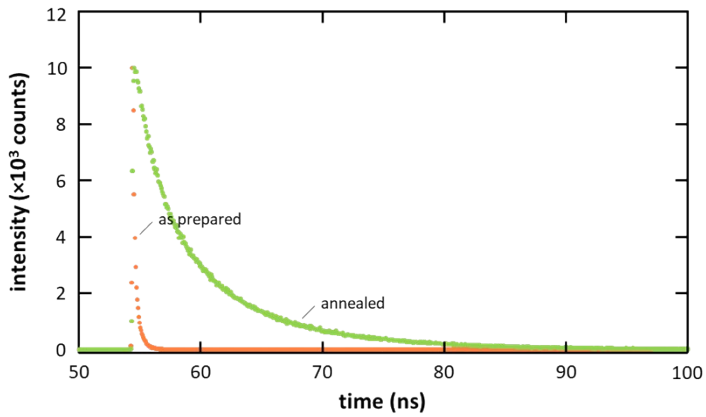


Fig. S7: Transient photoluminescence (TRPL) measurement for $\text{CsPb}(\text{I}_{0.67}\text{Br}_{0.33})_3$ thin films with and without post-annealing ($330\text{ }^\circ\text{C}$ for 1 min) after deposition. When fitted with a double-exponential function, charge carrier lifetimes of $\tau_1 = 0.19\text{ ns}$ and $\tau_2 = 0.81\text{ ns}$ with a weighted average value of $\tau_{\text{mean}} = 0.22\text{ ns}$ for the as-prepared thin film and $\tau_1 = 2.20\text{ ns}$ and $\tau_2 = 7.52\text{ ns}$ with a weighted average value of $\tau_{\text{mean}} = 4.90\text{ ns}$ for the annealed thin film are extracted, which indicates a significant improvement in thin-film quality during annealing. Both thin films were deposited on bare glass.

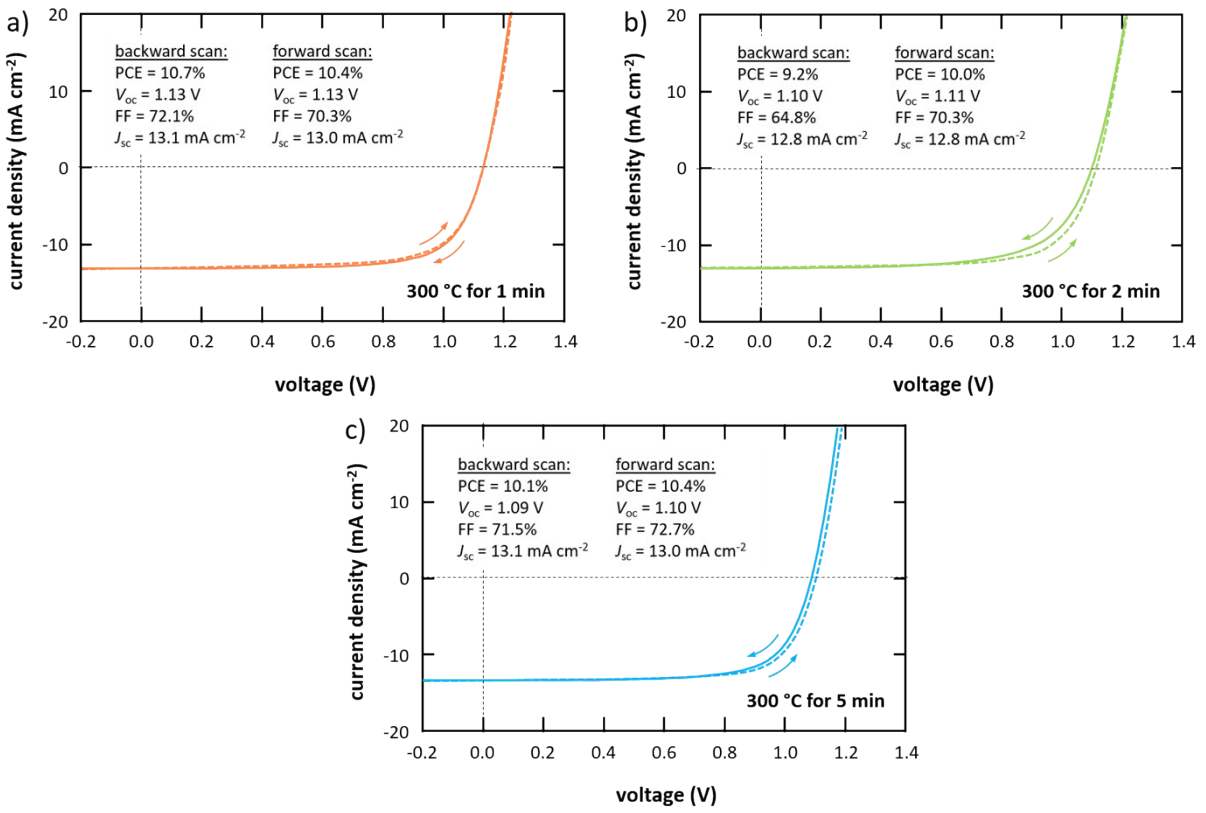


Fig. S8: Comparison of solar cell parameters of solar cells employing a $\text{CsPb}(\text{I}_{0.67}\text{Br}_{0.33})_3$ absorber annealed at 300°C for different times. Device performance is not significantly impacted whether the absorber films are annealed for (a) 1 min, (b) 2 min, or (c) 5 min.

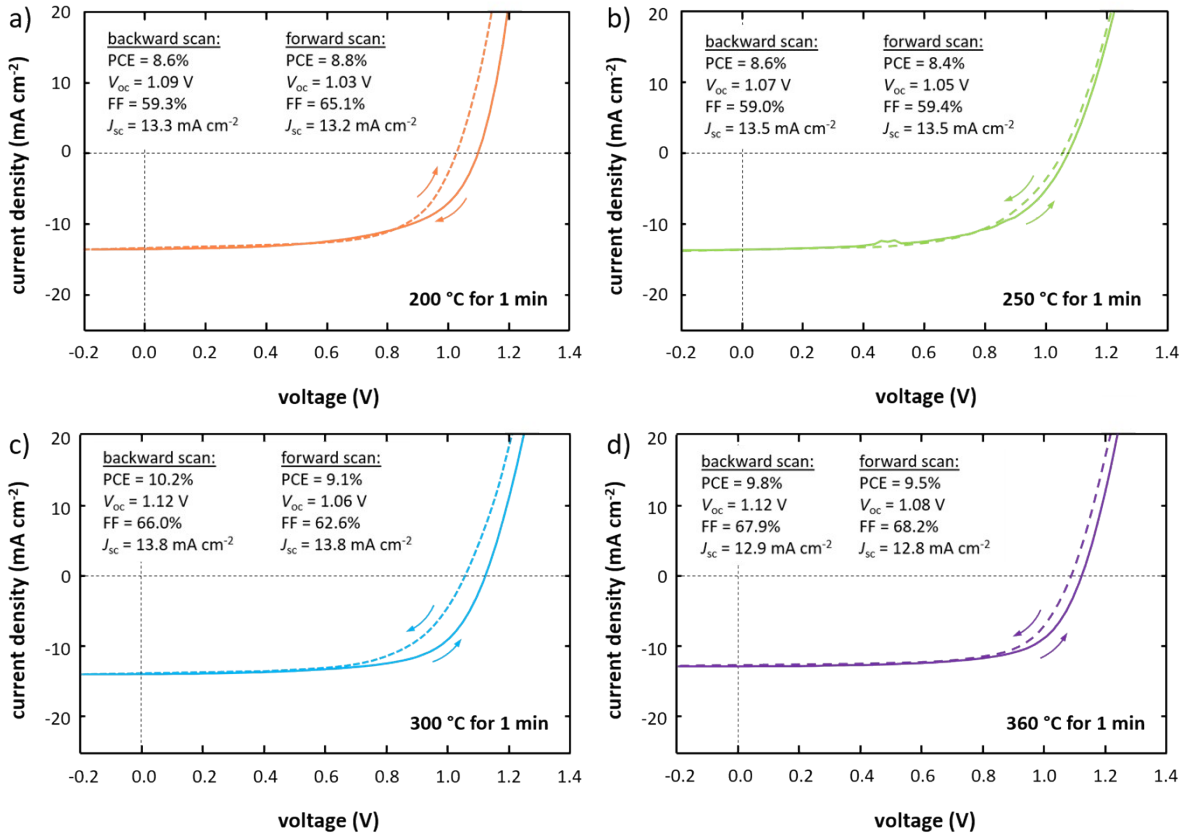


Fig. S9: Comparison of solar cell parameters of solar cells employing a $\text{CsPb}(\text{I}_{0.67}\text{Br}_{0.33})_3$ absorber annealed at (a) $200\text{ }^{\circ}\text{C}$, (b) $250\text{ }^{\circ}\text{C}$, (c) $300\text{ }^{\circ}\text{C}$, or (d) $360\text{ }^{\circ}\text{C}$ for 1 min. Good device performance is achieved for an annealing temperature of $300\text{ }^{\circ}\text{C}$.

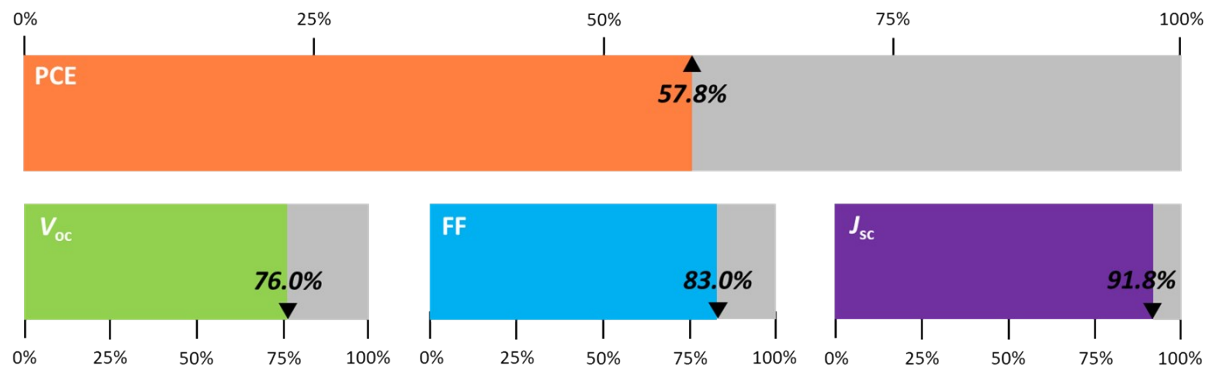


Fig. S10: Comparison of solar cell parameters of the best device fabricated by CFS in this work with the theoretical detailed-balance limit values. Values for the comparison are extracted from the reverse scan direction. For the detailed balance limit a bandgap for the $\text{CsPb}(\text{I}_{0.83}\text{Br}_{0.17})_3$ absorber of 1.86 eV was assumed. The main limitation in these devices is identified to be the open-circuit voltage followed by the fill factor.

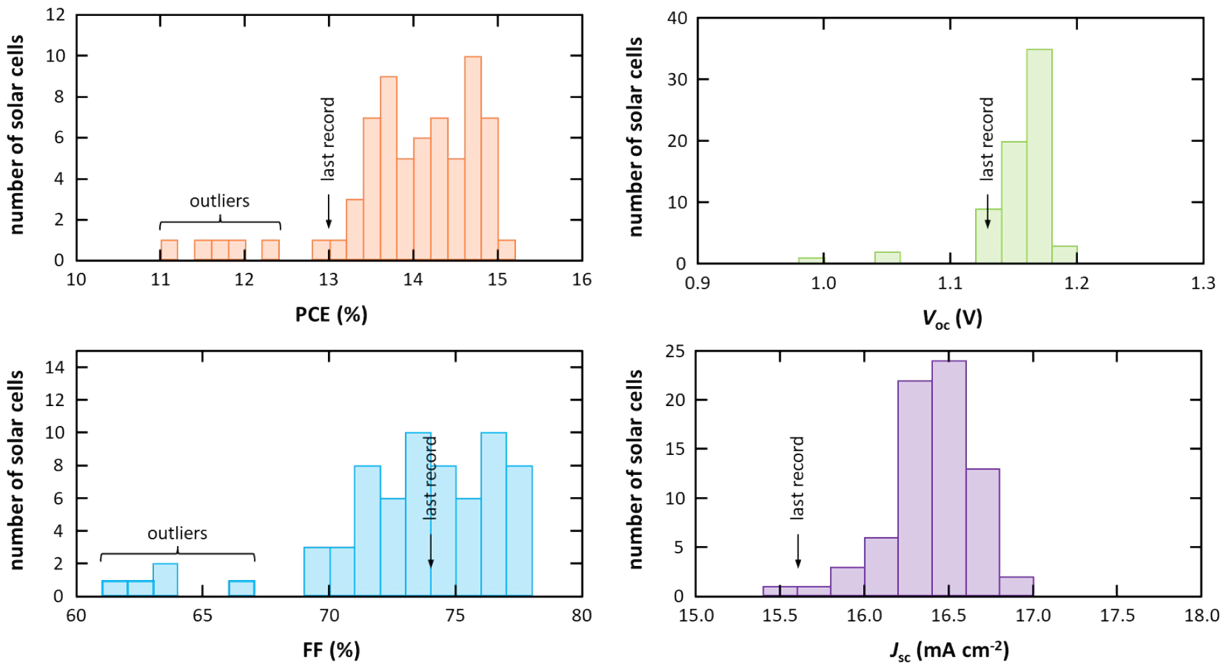


Fig. S11: Statistical distribution of solar cell parameters of solar cells with $\text{CsPb}(\text{I}_{0.83}\text{Br}_{0.17})_3$ absorbers prepared by CFS. Statistical data represents 78 solar cells on 13 substrates prepared in four individual evaporation runs employing two individually synthesized source powders. Best performing devices reach power conversion efficiencies as high as 15%. All devices outperform recent record values for vapor-processed inorganic perovskite solar cells significantly. The solar cell parameters were extracted from the reverse J - V scans. Obviously damaged solar cells have been removed from the histograms.

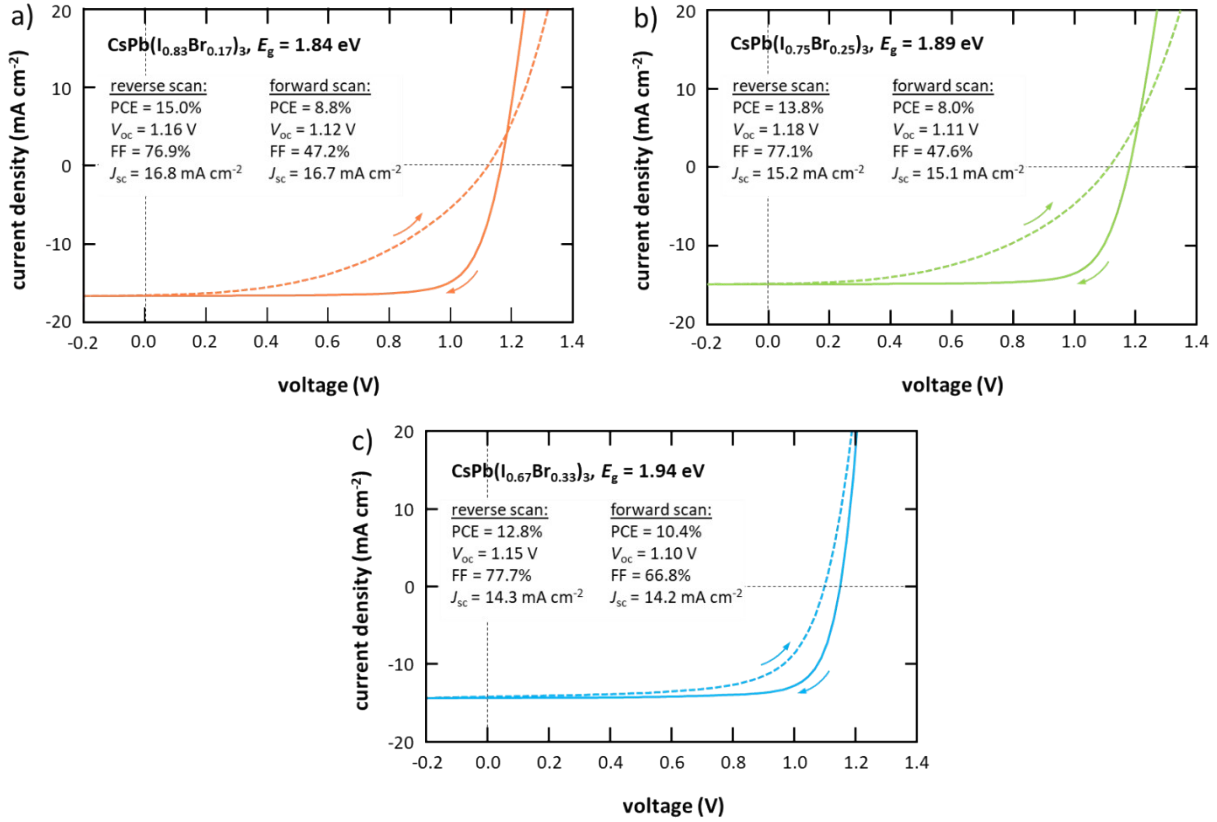


Fig. S12: Comparison of champion solar cells with different absorber compositions fabricated by CFS. The perovskite absorbers in these devices have a composition of (a) $\text{CsPb}(\text{I}_{0.83}\text{Br}_{0.17})_3$ ($E_g = 1.84 \text{ eV}$), (b) $\text{CsPb}(\text{I}_{0.75}\text{Br}_{0.25})_3$ ($E_g = 1.89 \text{ eV}$), or $\text{CsPb}(\text{I}_{0.67}\text{Br}_{0.33})_3$ ($E_g = 1.94 \text{ eV}$). Solar cells with the two lower-bandgap absorbers employ a cobalt TFSI salt doped spiro-MeOTAD while the absorber with the highest bandgap makes use of a classical oxygen doped spiro-MeOTAD, explaining the slightly lower hysteresis in this device (see Figure S11 in the Supporting Information).

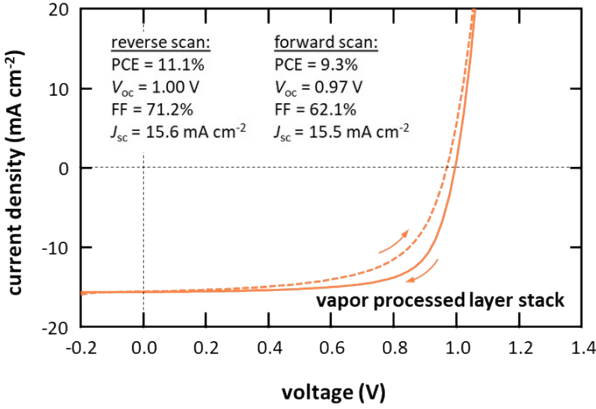


Fig. S13: Integration of absorbers prepared by CFS in a layer stack sequence employing only vapor-processed charge transport layers. The device architecture follows the layer stack sequence glass/ITO/NiO_x (20 nm)/PTAA (ca. 2 nm)/absorber/C₆₀ (25 nm)/BCP (6 nm)/Ag and employ a perovskite absorber with a composition of CsPb(I_{0.83}Br_{0.17})₃. The thin layer of solution-processed poly[bis(4-phenyl)-(2,4,6-trimethylphenyl)amine] (PTAA) is used as surface modification on top of the sputtered NiO_x hole transport layer. With a power conversion efficiency above 11% the device is currently the second most efficient solar cell employing a vapor processed inorganic perovskite absorber in inverted device architecture. Device performance is limited by the lower open-circuit voltage, which is a common issue for device architectures employing sputtered NiO_x layers, but hysteresis is significantly lower compared to devices employing spiro-MeOTAD as hole transport layer. For the fabrication of the sputtered NiO_x layer a sputter tool of Denton Vacuum LLC was used. The layer was sputtered at a process pressure of 25 mTorr with an argon-oxygen mixture as process gas at 60 W under rf-conditions from a two-inch NiO target (Kurt J. Lesker Company, 99.9% metallic purity). The substrates were not actively cooled or heated during the deposition and used as deposited. The electron transport layer consisting of C₆₀ and bathocuproine (BCP) was thermally evaporated.

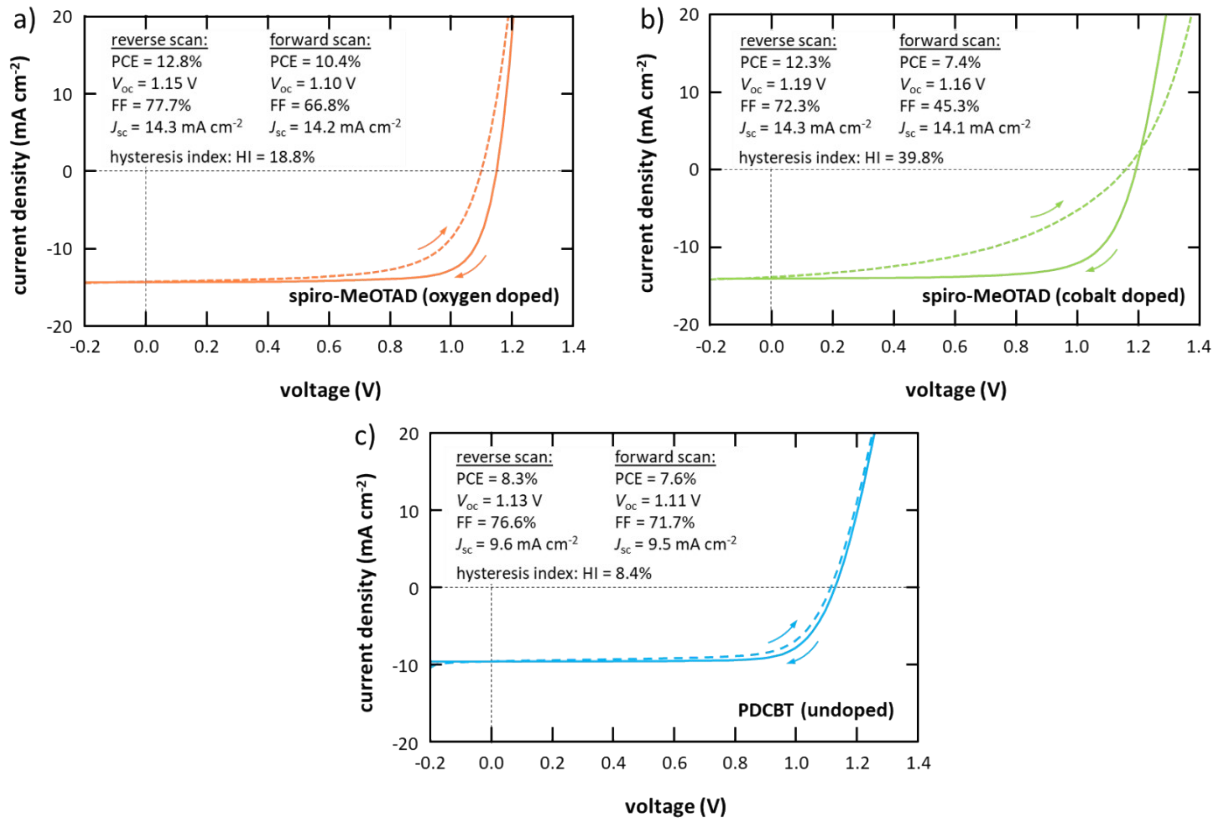


Fig. S14: Influence of the hole transport material (HTL) and doping mechanism on device performance and hysteresis in solar cells employing a $\text{CsPb}(\text{I}_{0.67}\text{Br}_{0.33})_3$ absorber. Typical J - V characteristic of solar cells with (a) an oxygen-doped spiro-MeOTAD, (b) a cobalt-doped spiro-MeOTAD, and (c) an undoped PDCBT hole transport layer. Hysteresis is significantly reduced in case of PDCBT while it is increased in case of a cobalt-doped spiro-MeOTAD, indicating an issue at the absorber/HTL interface to be the origin of the strong hysteresis in these devices. The hysteresis index HI is defined as $HI = (PCE_{rev} - PCE_{fwd}) \cdot PCE_{rev}^{-1}$. PDCBT was deposited in a hot casting approach with both the sample and the solution (10 mg/ml in a mixture of chlorobenzene and dichlorobenzene (1:1 vol.)) being kept at a temperature of 90 °C. Spin coating was performed at 1,000 rpm for 30 s in inert atmosphere without additional annealing or oxidation.

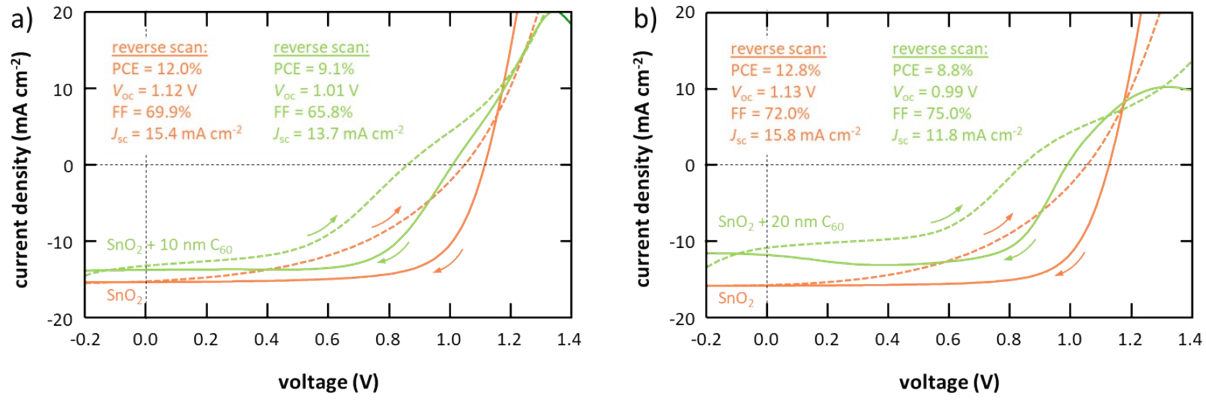


Fig. S15: Influence of a bilayer electron transport layer on the charge extraction and hysteresis. Comparisons of a bare SnO_2 electron transport layer and a $\text{SnO}_2/\text{C}_{60}$ bilayer electron transport layer with (a) a 10 nm thick C_{60} layer and (b) a 20 nm thick C_{60} layer. Extraction at the electron selective side of the layer stack is significantly hampered by the addition of a C_{60} layer, as can be concluded from the occurrence of a blocking behavior around the open-circuit point, the reduction of the open-circuit voltage, as well as the factitious shift of the maximum power point and fill factor toward higher current densities after the addition of C_{60} . This highlights again that issues at the interface between the hole transport layer and the absorber are the main root for the observed hysteresis. For this experiment, a $\text{CsPb}(\text{I}_{0.83}\text{Br}_{0.17})_3$ absorber with a cobalt-doped spiro-MeOTAD hole transport layer was used and C_{60} thermally evaporated on top of the SnO_2 electron transport layer.

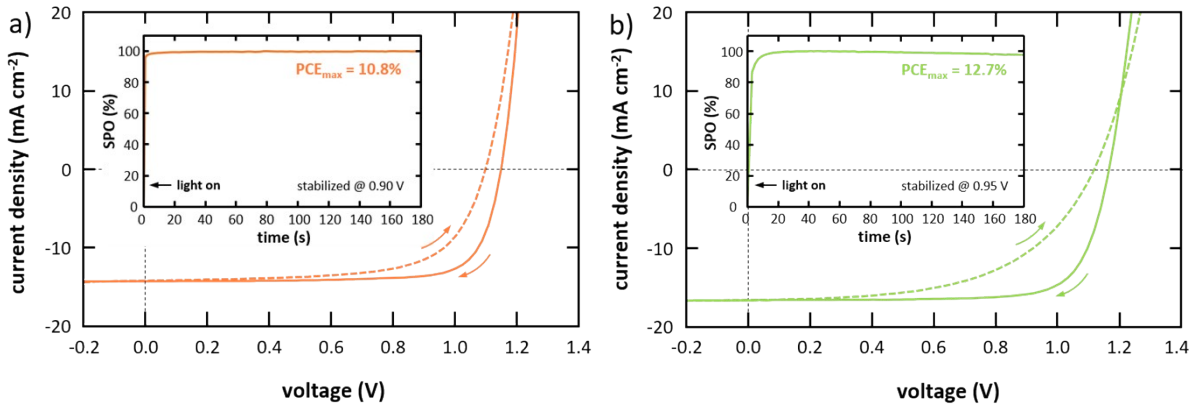


Fig. S16: Stabilized power output at constant voltage for the champion solar cell employing (a) a $\text{CsPb}(\text{I}_{0.67}\text{Br}_{0.33})_3$ or (b) $\text{CsPb}(\text{I}_{0.83}\text{Br}_{0.17})_3$ absorber prepared by CFS. A constant voltage of 0.9 or 0.95 V, which is close to the individual maximum power point (MPP) as extracted from the reverse J - V scan, was used for the measurements. Given the lower hysteresis in the device employing a $\text{CsPb}(\text{I}_{0.67}\text{Br}_{0.33})_3$ absorber (with an oxygen-doped spiro-MeOTAD, backward PCE from J - V scan 12.8%) stability is slightly better compared to the device employing a $\text{CsPb}(\text{I}_{0.83}\text{Br}_{0.17})_3$ (with a cobalt-doped spiro-MeOTAD, backward PCE from J - V scan 14.8%).

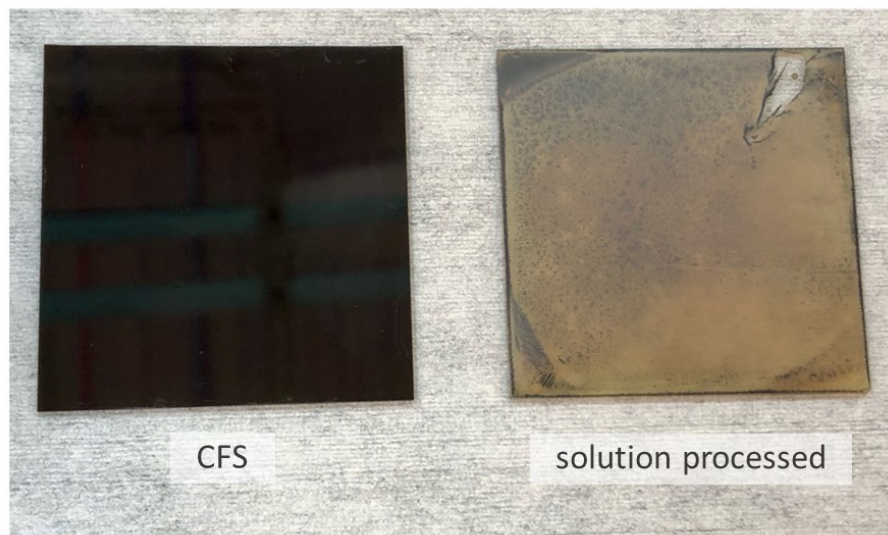


Fig. S17: Phase stability in ambient conditions (humidity < 20%) of a thin film prepared by CFS (left) and a solution-processed thin film (right) with the same composition of $\text{CsPb}(\text{I}_{0.67}\text{Br}_{0.33})_3$. After circa five hours in ambient conditions, the solution-processed thin film underwent nearly a complete phase change into the photoinactive phase, whereas the thin film prepared by CFS does not show any visual signs of a significant phase change.

Tab. S3: Summary of key characteristics of vapor-processed inorganic perovskite solar cell absorbers prepared by CFS with different deposition rates in this work. Data is presented visually in Figure 5 in the main manuscript.

absorber composition	deposition rate (nm min ⁻¹)	reverse scan direction				forward scan direction				doping
		PCE (%)	FF (%)	V _{oc} (V)	J _{sc} (mA cm ⁻²)	PCE (%)	FF (%)	V _{oc} (V)	J _{sc} (mA cm ⁻²)	
CsPb(I _{0.67} Br _{0.33}) ₃	95.0	12.8	77.7	1.15	14.3	10.4	66.8	1.10	14.2	oxygen-doped spiro-MeOTAD
CsPb(I _{0.75} Br _{0.25}) ₃	84.4	13.8	77.1	1.18	15.2	8.0	47.6	1.11	15.1	cobalt-doped spiro-MeOTAD
CsPb(I _{0.83} Br _{0.17}) ₃	66.7	14.1	74.0	1.16	16.5	7.7	42.3	1.11	16.4	cobalt-doped spiro-MeOTAD
CsPb(I _{0.83} Br _{0.17}) ₃	84.4	14.9	76.0	1.17	16.8	10.3	55.1	1.12	16.7	cobalt-doped spiro-MeOTAD
CsPb(I _{0.83} Br _{0.17}) ₃	87.3	13.3	70.9	1.16	16.2	7.2	39.8	1.12	16.1	cobalt-doped spiro-MeOTAD
CsPb(I _{0.83} Br _{0.17}) ₃	88.0	14.3	74.0	1.16	16.6	10.2	55.3	1.11	16.6	cobalt-doped spiro-MeOTAD
CsPb(I _{0.83} Br _{0.17}) ₃	95.0	14.1	71.6	1.15	17.1	9.3	50.3	1.08	16.9	cobalt-doped spiro-MeOTAD
CsPb(I _{0.83} Br _{0.17}) ₃	117.7	14.2	76.1	1.16	16.1	7.8	43.6	1.12	16.0	cobalt-doped spiro-MeOTAD
CsPb(I _{0.83} Br _{0.17}) ₃	127.2	14.1	76.5	1.15	16.0	7.4	41.9	1.11	15.9	cobalt-doped spiro-MeOTAD
CsPb(I _{0.83} Br _{0.17}) ₃	134.3	13.4	72.1	1.14	16.3	8.4	49.4	1.05	16.2	cobalt-doped spiro-MeOTAD

Notes on CFS and powder preparation

The CFS process allows materials with widely disparate vapor pressures to be deposited from a single source powder using the kinetics of rapid vaporization. Specifically, creating a ‘hot zone’ in which the powders reside for very short periods of time can allow for full vaporization without phase separation. Assuming a fixed material (i.e., inorganic halide perovskites) and a fixed system geometry (see Figure 2) the remaining variable is the powder particle size. The boat’s temperature for a successful deposition has both a lower and upper bound. The lower bound is easily determined as the temperature beneath which the least volatile component is not vaporized. For inorganic materials, the upper bound may seem limitless theoretically, but practically it is not. At a high enough temperature, the kinetic energy of the most volatile component relative to the least volatile component may cause phase separation in the gas phase due to the speed of the vaporized materials. We note that in our case we could not reach the upper bound due to equipment limitations.

Between these two bounds, the optimal temperature is a function of the largest particle size within the size distribution. As the largest particle size gets smaller the temperature required for full vaporization decreases and vice-versa as the largest particle size gets larger. As the particle size distribution increases it may be impossible to find a temperature at which the largest particles are fully vaporized without creating phase separation from the smallest particles in the distribution (i.e., both mean particle size and the size distribution are important). Finally, the mean particle size and size distribution also impact the powder feed rate and deposition rate. As the mean particle size increases the feed rate must be decreased so that the boat can maintain the optimal temperate as noted above. As the size distribution increases, the effective deposition rate fluctuates as a variety of different size particles are vaporized when coming into contact with the hot zone.

Given the above considerations, the optimal powders would be of the smallest mean size while maintaining a narrow distribution. Practically, powder processing would have to balance the effort required to produce ‘optimal’ powders with the deposition rates and resulting thin film quality required for the given process.

In the present study, we did experiment with different powder preparation by filtering the ball milled salts using a shaker/sieve and a series of sieves of 1000, 500, 250, 100, 40, and 20 μm meshes. We deposited the powders after the 250 μm and the 20 μm meshes and see no substantial difference in the resulting materials and devices.

References

- [1] M. Liu, M. B. Johnston, H. J. Snaith, *Nature* **2013**, *501*, 395.
- [2] M. R. Leyden, L. K. Ono, S. R. Raga, Y. Kato, S. Wang, Y. Qi, *J. Mater. Chem. A* **2014**, *2*, 18742.
- [3] C.-W. Chen, H.-W. Kang, S.-Y. Hsiao, P.-F. Yang, K.-M. Chiang, H.-W. Lin, *Adv. Mater.* **2014**, *26*, 6647.
- [4] L. K. Ono, S. Wang, Y. Kato, S. R. Raga, Y. Qi, *Energy Environ. Sci.* **2014**, *7*, 3989.
- [5] C. Roldán-Carmona, O. Malinkiewicz, A. Soriano, G. Mínguez Espallargas, A. García, P. Reinecke, T. Kroyer, M. I. Dar, M. K. Nazeeruddin, H. J. Bolink, *Energy Environ. Sci.* **2014**, *7*, 994.
- [6] C. Momblona, O. Malinkiewicz, C. Roldán-Carmona, A. Soriano, L. Gil-Escríg, E. Bandiello, M. Scheepers, E. Edri, H. J. Bolink, *APL Mater.* **2014**, *2*, 081504.
- [7] O. Malinkiewicz, A. Yella, Y. H. Lee, G. M. M. Espallargas, M. Graetzel, M. K. Nazeeruddin, H. J. Bolink, *Nat. Photonics* **2014**, *8*, 128.
- [8] O. Malinkiewicz, C. Roldán-Carmona, A. Soriano, E. Bandiello, L. Camacho, M. K. Nazeeruddin, H. J. Bolink, *Adv. Energy Mater.* **2014**, *4*, 1.
- [9] L. E. Polander, P. Pahner, M. Schwarze, M. Saalfrank, C. Koerner, K. Leo, *APL Mater.* **2014**, *2*, 1.
- [10] T. W. Ng, C. Y. Chan, M. F. Lo, Z. Q. Guan, C. S. Lee, *J. Mater. Chem. A* **2015**, *3*, 9081.
- [11] A. S. Subbiah, A. Halder, S. Ghosh, N. Mahuli, G. Hodes, S. K. Sarkar, *J. Phys. Chem. Lett.* **2014**, *5*, 1748.
- [12] H. Hu, D. Wang, Y. Zhou, J. Zhang, S. Lv, S. Pang, X. Chen, Z. Liu, N. P. Padture, G. Cui, *RSC Adv.* **2014**, *4*, 28964.
- [13] H. A. Abbas, R. Kottokkaran, B. Ganapathy, M. Samiee, L. Zhang, A. Kitahara, M. Noack, V. L. Dalal, *APL Mater.* **2015**, *3*.
- [14] J. Teuscher, A. Ulianov, O. Müntener, M. Grätzel, N. Tétreault, *ChemSusChem* **2015**, *8*, 3847.
- [15] S. Wang, L. K. Ono, M. R. Leyden, Y. Kato, S. R. Raga, M. V. Lee, Y. Qi, *J. Mater. Chem. A* **2015**, *3*, 14631.
- [16] M. M. Tavakoli, L. Gu, Y. Gao, C. Reckmeier, J. He, A. L. Rogach, Y. Yao, Z. Fan, *Sci. Rep.* **2015**, *5*, 1.
- [17] M. R. Leyden, M. V. Lee, S. R. Raga, Y. Qi, *J. Mater. Chem. A* **2015**, *3*, 16097.
- [18] P. Luo, Z. Liu, W. Xia, C. Yuan, J. Cheng, Y. Lu, *ACS Appl. Mater. Interfaces* **2015**, *7*, 2708.

- [19] D. Yang, Z. Yang, W. Qin, Y. Zhang, S. Liu, C. Li, *J. Mater. Chem. A* **2015**, *3*, 9401.
- [20] A. Ng, Z. Ren, Q. Shen, S. H. Cheung, H. C. Gokkaya, G. Bai, J. Wang, L. Yang, S. K. So, A. B. Djurišić, W. W. F. Leung, J. Hao, W. K. Chan, C. Surya, *J. Mater. Chem. A* **2015**, *3*, 9223.
- [21] G. Longo, L. Gil-Escríg, M. J. Degen, M. Sessolo, H. J. Bolink, *Chem. Commun.* **2015**, *51*, 7376.
- [22] M. R. Leyden, Y. Jiang, Y. Qi, *J. Mater. Chem. A* **2016**, *4*, 13125.
- [23] S. Y. Hsiao, H. L. Lin, W. H. Lee, W. L. Tsai, K. M. Chiang, W. Y. Liao, C. Z. Ren-Wu, C. Y. Chen, H. W. Lin, *Adv. Mater.* **2016**, *28*, 7013.
- [24] B. S. Kim, M. H. Choi, M. S. Choi, J. J. Kim, *J. Mater. Chem. A* **2016**, *4*, 5663.
- [25] C. Momblona, L. Gil-Escríg, E. Bandiello, E. M. Hutter, M. Sessolo, K. Lederer, J. Blochwitz-Nimoth, H. J. Bolink, *Energy Environ. Sci.* **2016**, *9*, 3456.
- [26] P. Fan, D. Gu, G. X. Liang, J. T. Luo, J. L. Chen, Z. H. Zheng, D. P. Zhang, *Sci. Rep.* **2016**, *6*, 1.
- [27] H. Xu, Y. Wu, F. Xu, J. Zhu, C. Ni, W. Wang, F. Hong, R. Xu, F. Xu, J. Huang, L. Wang, *RSC Adv.* **2016**, *6*, 48851.
- [28] J. Borchert, R. L. Milot, J. B. Patel, C. L. Davies, A. D. Wright, L. Mart, H. J. Snaith, L. M. Herz, M. B. Johnston, **2017**.
- [29] D. Forgács, L. Gil-Escríg, D. Pérez-Del-Rey, C. Momblona, J. Werner, B. Niesen, C. Ballif, M. Sessolo, H. J. Bolink, *Adv. Energy Mater.* **2017**, *7*, 1.
- [30] J. B. Patel, J. Wong-Leung, S. Van Reenen, N. Sakai, J. T. W. Wang, E. S. Parrott, M. Liu, H. J. Snaith, L. M. Herz, M. B. Johnston, *Adv. Electron. Mater.* **2017**, *3*, 1.
- [31] X. Zhu, D. Yang, R. Yang, B. Yang, Z. Yang, X. Ren, J. Zhang, J. Niu, J. Feng, S. Liu, *Nanoscale* **2017**, *9*, 12316.
- [32] M. M. Tavakoli, A. Simchi, X. Mo, Z. Fan, *Mater. Chem. Front.* **2017**, *1*, 1520.
- [33] L. Cojocaru, K. Wienands, T. W. Kim, S. Uchida, A. J. Bett, S. Rafizadeh, J. C. Goldschmidt, S. W. Glunz, *ACS Appl. Mater. Interfaces* **2018**, *10*, 26293.
- [34] G. Longo, C. Momblona, M. G. La-Placa, L. Gil-Escríg, M. Sessolo, H. J. Bolink, *ACS Energy Lett.* **2018**, *3*, 214.
- [35] D. Pérez-Del-Rey, P. P. Boix, M. Sessolo, A. Hadipour, H. J. Bolink, *J. Phys. Chem. Lett.* **2018**, *9*, 1041.
- [36] L. Gil-Escríg, C. Momblona, M. G. La-Placa, P. P. Boix, M. Sessolo, H. J. Bolink, *Adv. Energy Mater.* **2018**, *8*, 1.

- [37] L. Luo, Y. Zhang, N. Chai, X. Deng, J. Zhong, F. Huang, Y. Peng, Z. Ku, Y. B. Cheng, *J. Mater. Chem. A* **2018**, *6*, 21143.
- [38] M. Tai, X. Zhao, H. Wei, G. Wang, F. Hao, X. Li, X. Yin, Y. Zhou, J. Han, Y. Wei, K. Jiang, H. Lin, *ACS Appl. Mater. Interfaces* **2018**, *10*, 26206.
- [39] T. Abzieher, S. Moghadamzadeh, F. Schackmar, H. Eggers, F. Sutterlütii, A. Farooq, D. Kojda, K. Habicht, R. Schmager, A. Mertens, R. Azmi, L. Klohr, J. A. Schwenzer, M. Hetterich, U. Lemmer, B. S. Richards, M. Powalla, U. W. Paetzold, *Adv. Energy Mater.* **2019**, *9*, 1.
- [40] T. Abzieher, J. A. Schwenzer, S. Moghadamzadeh, F. Sutterluti, I. M. Hossain, M. Pfau, E. Lotter, M. Hetterich, B. S. Richards, U. Lemmer, M. Powalla, U. W. Paetzold, *IEEE J. Photovoltaics* **2019**, *9*, 1249.
- [41] J. Borchert, I. Levchuk, L. C. Snoek, M. U. Rothmann, R. Haver, H. J. Snaith, C. J. Brabec, L. M. Herz, M. B. Johnston, *ACS Appl. Mater. Interfaces* **2019**, *11*, 28851.
- [42] L. Qiu, S. He, Y. Jiang, D. Y. Son, L. K. Ono, Z. Liu, T. Kim, T. Bouloumis, S. Kazaoui, Y. Qi, *J. Mater. Chem. A* **2019**, *7*, 6920.
- [43] M. G. La-Placa, L. Gil-Escríg, D. Guo, F. Palazon, T. J. Savenije, M. Sessolo, H. J. Bolink, *ACS Energy Lett.* **2019**, *4*, 2893.
- [44] R. Kottokkaran, H. A. Gaonkar, H. A. Abbas, M. Noack, V. Dalal, *J. Mater. Sci. Mater. Electron.* **2019**, *30*, 5487.
- [45] J. M. Ball, L. Buizza, H. C. Sansom, M. D. Farrar, M. T. Klug, J. Borchert, J. Patel, L. M. Herz, M. B. Johnston, H. J. Snaith, *ACS Energy Lett.* **2019**, *4*, 2748.
- [46] D. Pérez-Del-Rey, L. Gil-Escríg, K. P. S. Zanoni, C. Dreessen, M. Sessolo, P. P. Boix, H. J. Bolink, *Chem. Mater.* **2019**, *31*, 6945.
- [47] F. Palazon, D. Pérez-del-Rey, B. Dänekamp, C. Dreessen, M. Sessolo, P. P. Boix, H. J. Bolink, *Adv. Mater.* **2019**, *31*.
- [48] D. Kiermasch, L. Gil-Escríg, A. Baumann, H. J. Bolink, V. Dyakonov, K. Tvingstedt, *J. Mater. Chem. A* **2019**, *7*, 14712.
- [49] D. Lin, T. Zhang, J. Wang, M. Long, F. Xie, J. Chen, B. Wu, T. Shi, K. Yan, W. Xie, P. Liu, J. Xu, *Nano Energy* **2019**, *59*, 619.
- [50] M. T. Hoerantner, E. L. Wassweiler, H. Zhang, A. Panda, M. Nasilowski, A. Osherov, R. Swartwout, A. E. Driscoll, N. S. Moody, M. G. Bawendi, K. F. Jensen, V. Bulović, *ACS Appl. Mater. Interfaces* **2019**, *11*, 32928.
- [51] V. Arivazhagan, J. Xie, Z. Yang, P. Hang, M. M. Parvathi, K. Xiao, C. Cui, D. Yang, X. Yu, *Sol. Energy* **2019**, *181*, 339.

- [52] M. M. Tavakoli, P. Yadav, D. Prochowicz, R. Tavakoli, M. Saliba, *J. Phys. D. Appl. Phys.* **2019**, *52*.
- [53] H. Peng, Z. Su, Z. Zheng, H. Lan, J. Luo, P. Fan, **2019**.
- [54] Z. H. Zheng, H. Bin Lan, Z. H. Su, H. X. Peng, J. T. Luo, G. X. Liang, P. Fan, *Sci. Rep.* **2019**, *9*, 1.
- [55] L. Qiu, S. He, Z. Liu, L. K. Ono, D. Y. Son, Y. Liu, G. Tong, Y. Qi, *J. Mater. Chem. A* **2020**, *8*, 23404.
- [56] S. Ngqoloda, C. J. Arendse, T. F. Muller, P. F. Miceli, S. Guha, L. Mostert, C. J. Oliphant, *ACS Appl. Energy Mater.* **2020**, *3*, 2350.
- [57] T. Hellmann, C. Das, T. Abzieher, J. A. Schwenzer, M. Wussler, R. Dachauer, U. W. Paetzold, W. Jaegermann, T. Mayer, *Adv. Energy Mater.* **2020**, *10*.
- [58] A. J. Harding, A. G. Kuba, B. E. McCandless, U. K. Das, K. D. Dobson, B. A. Ogunnaike, W. N. Shafarman, *RSC Adv.* **2020**, *10*, 16125.
- [59] K. B. Lohmann, J. B. Patel, M. U. Rothmann, C. Q. Xia, R. D. J. Oliver, L. M. Herz, H. J. Snaith, M. B. Johnston, *ACS Energy Lett.* **2020**, *5*, 710.
- [60] J. Li, H. A. Dewi, H. Wang, J. H. Lew, N. Mathews, S. Mhaisalkar, A. Bruno, *Sol. RRL* **2020**, *4*, 1.
- [61] M. Roß, L. Gil-Escríg, A. Al-Ashouri, P. Tockhorn, M. Jošt, B. Rech, S. Albrecht, *ACS Appl. Mater. Interfaces* **2020**, *12*, 39261.
- [62] L. Gil-Escríg, C. Dreessen, I. C. Kaya, B. S. Kim, F. Palazon, M. Sessolo, H. J. Bolink, *ACS Energy Lett.* **2020**, *5*, 3053.
- [63] A. Babaei, W. Soltanpoor, M. A. Tesa-Serrate, S. Yerci, M. Sessolo, H. J. Bolink, *Energy Technol.* **2020**, *8*, 1.
- [64] B. S. Kim, L. Gil-Escríg, M. Sessolo, H. J. Bolink, *J. Phys. Chem. Lett.* **2020**, *11*, 6852.
- [65] J. Li, H. Wang, X. Y. Chin, H. A. Dewi, K. Vergeer, T. W. Goh, J. W. M. Lim, J. H. Lew, K. P. Loh, C. Soci, T. C. Sum, H. J. Bolink, N. Mathews, S. Mhaisalkar, A. Bruno, *Joule* **2020**, *4*, 1035.
- [66] K. P. S. Zanoni, D. Pérez-del-Rey, C. Dreessen, A. Ma, A. S. S. de Camargo, M. Sessolo, P. P. Boix, H. J. Bolink, *Energy Technol.* **2020**, *8*, 1.
- [67] A. Babaei, K. P. S. Zanoni, L. Gil-Escríg, D. Pérez-del-Rey, P. P. Boix, M. Sessolo, H. J. Bolink, *Front. Chem.* **2020**, *7*, 1.
- [68] A. M. Igual-Muñoz, J. Ávila, P. P. Boix, H. J. Bolink, *Sol. RRL* **2020**, *4*, 1.
- [69] Y. H. Chiang, M. Anaya, S. D. Stranks, *ACS Energy Lett.* **2020**, *5*, 2498.

- [70] R. Ji, Z. Zhang, C. Cho, Q. An, F. Paulus, M. Kroll, M. Löffler, F. Nehm, B. Rellinghaus, K. Leo, Y. Vaynzof, *J. Mater. Chem. C* **2020**, *8*, 7725.
- [71] T. Lei, F. Li, X. Zhu, H. Dong, Z. Niu, S. Ye, W. Zhao, J. Xi, B. Jiao, L. Ding, Z. Wu, *Sol. RRL* **2020**, *2000292*, 1.
- [72] E. Smecca, V. Valenzano, S. Valastro, I. Deretzis, G. Mannino, G. Malandrino, G. Accorsi, S. Colella, A. Rizzo, A. La Magna, A. Listorti, A. Alberti, *J. Mater. Chem. A* **2021**, *9*, 16456.
- [73] F. Sahli, N. Miaz, N. Salsi, C. Bucher, A. Schafflützel, Q. Guesnay, L. Duchêne, B. Niesen, C. Ballif, Q. Jeangros, *ACS Appl. Energy Mater.* **2021**, *4*, 4333.
- [74] Y. Choi, D. Koo, M. Jeong, G. Jeong, J. Lee, B. Lee, K. J. Choi, C. Yang, H. Park, *Sol. RRL* **2021**, *5*, 1.
- [75] J. Li, H. A. Dewi, H. Wang, J. Zhao, N. Tiwari, N. Yantara, T. Malinauskas, V. Getautis, T. J. Savenije, N. Mathews, S. Mhaisalkar, A. Bruno, *Adv. Funct. Mater.* **2021**, *31*.
- [76] H. A. Dewi, J. Li, H. Wang, B. Chaudhary, N. Mathews, S. Mhaisalkar, A. Bruno, *Adv. Funct. Mater.* **2021**, *31*, DOI 10.1002/adfm.202100557.
- [77] A. Paliwal, C. Dreessen, K. P. S. Zanoni, B. Dänekamp, B. S. Kim, M. Sessolo, K. Vandewal, H. J. Bolink, *ACS Photonics* **2021**, *8*, 2067.
- [78] I. Susic, K. P. S. Zanoni, A. Paliwal, I. C. Kaya, Z. Hawash, M. Sessolo, E. Moons, H. J. Bolink, *Sol. RRL* **2022**, *6*.
- [79] L. Gil-Escríg, M. Roß, J. Sutter, A. Al-Ashouri, C. Becker, S. Albrecht, *Sol. RRL* **2021**, *5*, 1.
- [80] N. Klipfel, C. Momblona, H. Kanda, N. Shibayama, Y. Nakamura, M. D. Mensi, C. Liu, C. Roldán-Carmona, M. K. Nazeeruddin, *Sol. RRL* **2021**, *5*.
- [81] T. Gallet, R. G. Poeira, E. M. Lanzoni, T. Abzieher, U. W. Paetzold, A. Redinger, *ACS Appl. Mater. Interfaces* **2021**, *13*, 2642.
- [82] M. Roß, S. Severin, M. B. Stutz, P. Wagner, H. Köbler, M. Favin-Lévéque, A. Al-Ashouri, P. Korb, P. Tockhorn, A. Abate, B. Stannowski, B. Rech, S. Albrecht, *Adv. Energy Mater.* **2021**, *11*.
- [83] I. C. Kaya, K. P. S. Zanoni, F. Palazon, M. Sessolo, H. Akyildiz, S. Sonmezoglu, H. J. Bolink, *Adv. Energy Sustain. Res.* **2021**, *2*, 2000065.
- [84] J. Feng, Y. Jiao, H. Wang, X. Zhu, Y. Sun, M. Du, Y. Cao, D. Yang, S. F. Liu, *Energy Environ. Sci.* **2021**, *14*, 3035.
- [85] L. Gil-Escríg, C. Dreessen, F. Palazon, Z. Hawash, E. Moons, S. Albrecht, M. Sessolo, H. J. Bolink, *ACS Energy Lett.* **2021**, *6*, 827.

- [86] T. Abzieher, T. Feeney, F. Schackmar, Y. J. Donie, I. M. Hossain, J. A. Schwenzer, T. Hellmann, T. Mayer, M. Powalla, U. W. Paetzold, *Adv. Funct. Mater.* **2021**, *31*.
- [87] D. B. Ritzer, T. Abzieher, A. Basibüyük, T. Feeney, F. Laufer, S. Ternes, B. S. Richards, S. Bergfeld, U. W. Paetzold, *Prog. Photovoltaics Res. Appl.* **2022**, *30*, 360.
- [88] D. Lin, X. Xu, T. Zhang, N. Pang, J. Wang, H. Li, T. Shi, K. Chen, Y. Zhou, X. Wang, J. Xu, P. Liu, W. Xie, *Nano Energy* **2021**, *84*, 105893.
- [89] M. Kroll, S. D. Öz, Z. Zhang, R. Ji, T. Schramm, T. Antrack, Y. Vaynzof, S. Olthof, K. Leo, *Sustain. Energy Fuels* **2022**, 3230.
- [90] H. Li, J. Zhou, L. Tan, M. Li, C. Jiang, S. Wang, X. Zhao, *Sci. Adv.* **2022**, *8*, 1.
- [91] Q. Ma, S. Huang, X. Wen, M. A. Green, A. W. Y. Ho-Baillie, *Adv. Energy Mater.* **2016**, *6*, 2.
- [92] D. Moghe, L. Wang, C. J. Traverse, A. Redoute, M. Sponseller, P. R. Brown, V. Bulović, R. R. Lunt, *Nano Energy* **2016**, *28*, 469.
- [93] Q. Ma, S. Huang, S. Chen, M. Zhang, C. F. J. Lau, M. N. Lockrey, H. K. Mulmudi, Y. Shan, J. Yao, J. Zheng, X. Deng, K. Catchpole, M. A. Green, A. W. Y. Ho-Baillie, *J. Phys. Chem. C* **2017**, *121*, 19642.
- [94] M. Shahiduzzaman, K. Yonezawa, K. Yamamoto, T. S. Ripolles, M. Karakawa, T. Kuwabara, K. Takahashi, S. Hayase, T. Taima, *ACS Omega* **2017**, *2*, 4464.
- [95] E. M. Hutter, R. J. Sutton, S. Chandrashekhar, M. Abdi-Jalebi, S. D. Stranks, H. J. Snaith, T. J. Savenije, *ACS Energy Lett.* **2017**, *2*, 1901.
- [96] C. Y. Chen, H. Y. Lin, K. M. Chiang, W. L. Tsai, Y. C. Huang, C. S. Tsao, H. W. Lin, *Adv. Mater.* **2017**, *29*.
- [97] M. Chen, M. G. Ju, A. D. Carl, Y. Zong, R. L. Grimm, J. Gu, X. C. Zeng, Y. Zhou, N. P. Padture, *Joule* **2018**, *2*, 558.
- [98] J. Lei, F. Gao, H. Wang, J. Li, J. Jiang, X. Wu, R. Gao, Z. Yang, S. (Frank) Liu, *Sol. Energy Mater. Sol. Cells* **2018**, *187*, 1.
- [99] R. Kottokkaran, H. A. Gaonkar, B. Bagheri, V. L. Dalal, *J. Vac. Sci. Technol. A* **2018**, *36*, 041201.
- [100] H. Li, G. Tong, T. Chen, H. Zhu, G. Li, Y. Chang, L. Wang, Y. Jiang, *J. Mater. Chem. A* **2018**, *6*, 14255.
- [101] C.-G. Park, W.-G. Choi, S. Na, T. Moon, *Electron. Mater. Lett.* **2019**, *15*, 56.
- [102] W. Chen, J. Zhang, G. Xu, R. Xue, Y. Li, Y. Zhou, J. Hou, Y. Li, *Adv. Mater.* **2018**, *30*.
- [103] P. Fan, H.-X. Peng, Z.-H. Zheng, Z.-H. Chen, S.-J. Tan, X.-Y. Chen, Y.-D. Luo, Z.-H. Su, J.-T. Luo, G.-X. Liang, *Nanomaterials* **2019**, *9*, 1.

- [104] G. Tong, T. Chen, H. Li, L. Qiu, Z. Liu, Y. Dang, W. Song, L. K. Ono, Y. Jiang, Y. Qi, *Nano Energy* **2019**, *65*, 104015.
- [105] T. Chen, G. Tong, E. Xu, H. Li, P. Li, Z. Zhu, J. Tang, Y. Qi, Y. Jiang, *J. Mater. Chem. A* **2019**, *7*, 20597.
- [106] H. Y. Lin, C. Y. Chen, B. W. Hsu, Y. L. Cheng, W. L. Tsai, Y. C. Huang, C. S. Tsao, H. W. Lin, *Adv. Funct. Mater.* **2019**, *29*.
- [107] P. Becker, J. A. Márquez, J. Just, A. Al-Ashouri, C. Hages, H. Hempel, M. Jošt, S. Albrecht, R. Frahm, T. Unold, *Adv. Energy Mater.* **2019**, *9*, 16.
- [108] X. Liu, X. Tan, Z. Liu, B. Sun, J. Li, S. Xi, T. Shi, G. Liao, *J. Power Sources* **2019**, *443*, 227269.
- [109] Y. Zhang, L. Luo, J. Hua, C. Wang, F. Huang, J. Zhong, Y. Peng, Z. Ku, Y. bing Cheng, *Mater. Sci. Semicond. Process.* **2019**, *98*, 39.
- [110] M. Tai, G. Wang, X. Yin, Y. Zhou, J. Han, Y. Wei, K. Jiang, H. Lin, *Energy Technol.* **2019**, *7*, 1.
- [111] J. Li, R. Gao, F. Gao, J. Lei, H. Wang, X. Wu, J. Li, H. Liu, X. Hua, S. (Frank) Liu, *J. Alloys Compd.* **2020**, *818*.
- [112] H. Gaonkar, J. Zhu, R. Kottokkaran, B. Bhageri, M. Noack, V. Dalal, *ACS Appl. Energy Mater.* **2020**, *3*, 3497.
- [113] L. Mi, Y. Zhang, T. Chen, E. Xu, Y. Jiang, *RSC Adv.* **2020**, *10*, 12298.
- [114] A. M. Igual-Muñoz, J. Navarro-Alapont, C. Dreessen, F. Palazon, M. Sessolo, H. J. Bolink, *Chem. Mater.* **2020**, *32*, 8641.
- [115] T. Xiang, Y. Zhang, H. Wu, J. Li, L. Yang, K. Wang, J. Xia, Z. Deng, J. Xiao, W. Li, Z. Ku, F. Huang, J. Zhong, Y. Peng, Y. B. Cheng, *Sol. Energy Mater. Sol. Cells* **2020**, *206*, 110317.
- [116] J. Hua, X. Deng, C. Niu, F. Huang, Y. Peng, W. Li, Z. Ku, Y. bing Cheng, *RSC Adv.* **2020**, *10*, 8905.
- [117] M. H. Abib, J. Li, H. Yang, M. Wang, T. Chen, E. Enzexu, Y. Jiang, *RSC Adv.* **2021**, *11*, 3380.
- [118] Y. Duan, G. Zhao, X. Liu, J. Ma, S. Chen, Y. Song, X. Pi, X. Yu, D. Yang, Y. Zhang, F. Guo, *Appl. Surf. Sci.* **2021**, *562*, 150153.
- [119] L. Liu, S. E. Yang, P. Liu, Y. Chen, *Sol. Energy* **2022**, *232*, 320.